Pyruvate dehydrogenase kinase supports macrophage NLRP3 inflammasome activation during acute inflammation

Allison K. Meyers [1], Zhan Wang [2, 6], Wenzheng Han [2, 3, 6], Qingxia Zhao [2, 6], Manal Zabalawi [2], Juan Liu [4], Rajesh K Manne [5], Hui-Kuan Lin [5], Cristina M. Furdui [2], Jason W. Locasale [4], Charles E. McCall [1, 2], Xuewei Zhu [1, 2, 7, *]

[1.] Department of Microbiology and Immunology, Wake Forest School of Medicine, Winston-Salem, NC 27157, USA.

[2.] Department of Internal Medicine, Section on Molecular Medicine, Wake Forest School of Medicine, Winston-Salem, NC 27157, USA.

[3.] Department of Cardiology, Huadong Hospital Affiliated to Fudan University, Shanghai, 200040, China.

[4.] Department of Pharmacology and Cancer Biology, Duke University School of Medicine, Durham, NC 27710, USA.

[5.] Department of Cancer Biology, Wake Forest School of Medicine, Winston-Salem, NC 27157, USA.

[6.] These authors contributed equally to this work.

[7.] Lead Contact.

* Correspondence: xwzhu@wakehealth.edu

Summary

Activating macrophage NLRP3 inflammasome can promote excessive inflammation, leading to severe cell and tissue damage and organ dysfunction. Here, we showed that pharmacological or genetic inhibition of pyruvate dehydrogenase kinase (PDHK) significantly attenuated macrophage NLRP3 inflammasome activation. Broad rewiring of intracellular metabolism and enhanced autophagic flux occurred in inflammasome-activated macrophages, but neither was necessary for the PDHK-regulated reduction of NLRP3 inflammasome activity. PDHK inhibition protected against inflammation-induced mitochondrial fragmentation and cristae remodeling and improved mitochondrial function by repurposing mitochondria from ROS production to ATP generation. Inhibition of PDHK increased the expression of the mitochondrial fusion protein optic atrophy-1 (OPA1). Suppression of OPA1 partially reversed the effect of PDHK inhibition on NLRP3 inflammasome activation. In conclusion, our study suggests that inhibition of PDHK dampens macrophage NLRP3 inflammasome activation during acute inflammation by ameliorating mitochondrial damage in a mechanism separate from its canonical role as a metabolic regulator.

Keywords

NLRP3 inflammasome, macrophages, sepsis, pyruvate dehydrogenase kinase, immunometabolism, mitochondria, cristae, autophagy, mitochondrial fission and fusion

Introduction

Sepsis is a life-threatening organ dysfunction syndrome caused by a dysregulated host response to infection, characterized by inflammation, cell death, and organ failure. Macrophages play essential roles throughout all phases of sepsis (Stearns-Kurosawa et al., 2011, Wiersinga et al., 2014). In sensing and promoting inflammation from diverse environmental threats, macrophages express pattern recognition receptors, including toll-like receptors (TLRs) and intracellular NOD-like receptors, such as NOD-, LRP-, and pyrin domain-containing protein 3 (NLRP3). Activation of NLRP3 results in assembly and activation of the NLRP3 inflammasome, a large multimeric cytosolic protein complex composed of NLRP3, caspase-1, and ASC. In general, activation of NLRP3 inflammasome in macrophages requires two-step signaling: priming and complex assembly (Lamkanfi and Dixit, 2014, Henao-Mejia et al., 2014, Rathinam et al., 2012a, Lamkanfi and Dixit, 2012, Swanson et al., 2019, Mangan et al., 2018). The priming step (signal 1) is triggered by TLR activation, for example, lipopolysaccharide (LPS)-induced TLR4 activation. The complex assembly step (signal 2) can be activated by a wide range of stimuli, including ATP, pore-forming toxin, and particulates (Lamkanfi and Dixit, 2014, Henao-Mejia et al., 2014, Rathinam et al., 2012a, Lamkanfi and Dixit, 2012), leading to self-cleavage of caspase-1, processing of proinflammatory cytokines IL-1β and IL-18, and pyroptotic cell death (pyroptosis) (Kayagaki et al., 2013, Hagar et al., 2013, Aachoui et al., 2013, Rathinam et al., 2012b, Broz et al., 2012, Kayagaki et al., 2011). Macrophage NLRP3 inflammasomal response is critical for host defense against invading microbes (Broz et al., 2010, Fang et al., 2011). However, excessive NLRP3 inflammasome activation exacerbates tissue inflammation, cell death, and organ damage, accelerating the pathogenesis of many inflammatory diseases, including cardiovascular disease, type II diabetes, sepsis, and COVID-19 (Ferreira et al., 2021, Meyers and Zhu, 2020). To date, how the NLRP3 inflammasome is activated and deactivated during inflammation is still not well understood. Uncovering the underlying mechanisms of NLRP3 inflammasome activation is valuable and fundamental as they may lead to novel therapeutic strategies for preventing and treating inflammatory diseases.

In the past decade, the rapid growth of the immunometabolism and mitochondrial bioenergetics fields highlight that cellular metabolism tightly regulates the function, activation, and deactivation of inflammatory cells, including macrophages (Pearce and Pearce, 2013, Kelly and O'Neill, 2015, O'Neill et al., 2016). Interestingly, metabolic stress, such as dysregulated glycolysis (Moon et al., 2015a, Wolf et al., 2016, Xie et al., 2016) or dysfunctional Krebs cycle (or TCA cycle) (Tannahill et al., 2013, Moon et al., 2015b, Mills et al., 2016), or mitochondrial oxidative stress, have been demonstrated to activate the NLRP3 inflammasome. In view of this, mitochondria play a central role in regulating the NLRP3 inflammasome activation by controlling TCA cycle intermediate and energy production and acting as a source of inflammasome activators or deactivators. For example, dysfunctional mitochondria release mitochondrial reactive oxygen species (mtROS) (Zhou et al., 2011, Cruz et al., 2007) and newly synthesized mitochondrial DNA (Nakahira et al., 2011, Shimada et al., 2012), or expose inner membrane cardiolipin on the outer membrane to activate the NLRP3 inflammasome (Iyer et al., 2013). Moreover, TCA cycle intermediates succinate (Mills et al., 2016, Tannahill et al., 2013), itaconate (Bambouskova

et al., 2021, Swain et al., 2020, Hooftman et al., 2020), and fumarate (Humphries et al., 2020) differentially regulate NLRP3 inflammasome activation. Despite the existing studies, our knowledge is still limited regarding the biology and mechanisms of metabolic regulation of NLRP3 inflammasome activation.

Mitochondrial pyruvate dehydrogenase (PDH) complex (PDC) is the gate-keeping and rate-limiting enzyme for mitochondrial glucose oxidation via decarboxylation of pyruvate to acetyl-CoA, a mitochondrial oxidation fuel (Stacpoole, 2012). The PDH phosphorylation state highly influences the activities of PDC. Pyruvate dehydrogenase kinase (PDHK isoforms 1-4) reversibly phosphorylates the PDHe1α subunit and inhibits PDC, whereas pyruvate dehydrogenase phosphatase (PDP) dephosphorylates and activates PDC (Patel et al., 2014, Klyuyeva et al., 2019, Karpova et al., 2003, Stacpoole, 2012). PDHK promotes macrophage polarization to the classically-activated or M1 phenotype (Min et al., 2019) and is a negative regulator of anti-inflammatory cytokine IL-10 production in macrophages (Na et al., 2020). Interestingly, pyruvate dehydrogenase kinase 1 (PDHK1) is persistently expressed in monocytes and macrophages in septic mice and human blood monocytes (Liu et al., 2012). The targeting of PDHK with its prototypic inhibitor dichloroacetate (DCA), a structural analog of pyruvate (the endogenous inhibitor of PDHK) (Stacpoole, 2012), protected mice against cecal-ligation and puncture (CLP)-induced polymicrobial infection (McCall et al., 2018). However, the molecular mechanism underlying DCA-induced septic protection and its relation to the regulation of the NLRP3 inflammasome is unclear.

Given the fundamental role of macrophage NLRP3 inflammasome dysregulation in the pathogenesis of sepsis, here, we sought to understand whether, to what extent, and how PDHK regulates NLRP3 inflammasome activation and cell death in macrophages. We demonstrate that inhibition of PDHK reducescaspase-1 cleavage in blood monocytes and neutrophils and lowers the circulating level of IL-1β in septic mice, and likewise that pharmacological or genetic inhibition of PDHK *in vitro* suppresses macrophage NLRP3 inflammasome activation. Furthermore, we found that PDHK inhibition protects against mitochondrial fragmentation, preserves mitochondrial ultrastructure, and favors ATP production over ROS generation. Unexpectedly, the suppressive effect of PDHK inhibition on the NLRP3 inflammasome is independent of PDH or autophagic flux. Our study uncovers a non-canonical role for mitochondrial PDHK in supporting mitochondrial oxidative stress to drive NLRP3 inflammasome activation during acute inflammation. PDHK may be a promising therapeutic target for preventing and treating inflammatory diseases caused by uncontrolled NLRP3 inflammasome activation.

Results

PDHK inhibition lowers plasma IL-1β and blood monocyte caspase-1 activity in septic mice

Previous studies of murine sepsis demonstrate that *in vivo* targeting of PDHK with DCA, administered as a single dose of 25 mg/kg 24 h post cecal ligation and puncture (CLP), significantly improves survival of septic mice (McCall et al., 2018). However, the molecular mechanism supporting survival was less clear. As macrophage NLRP3 inflammasome plays a critical role in the pathogenesis of sepsis, we asked whether DCA regulates NLRP3 inflammasome activation during sepsis. To test this, we first analyzed the plasma concentration of IL-1β, one of the end-products of the NLRP3 inflammasome activation, in mice with sham-operation control, CLP-induced sepsis, and DCA-treated septic mice. DCA (25 mg/kg) was given to septic mice 24 h post CLP for 6 h, as reported previously and depicted in **Figure 1A** (McCall et al., 2018). We found that CLP-induced septic mice showed a significantly elevated IL-1β concentration in plasma relative to sham control (**Figure 1B**). CLP mice also displayed monocytosis and neutrophilia, as demonstrated by a higher percentage of monocytes (identified as $CD115^{+}Ly6G^{-}$) and neutrophils ($CD115^{-}Ly6G^{+}$) (**Figures 1C-1E**) in peripheral blood circulation, further suggesting a hyper-inflammatory state in the septic mice. Moreover, we observed elevated activities of caspase-1 (caspase-1 cleavage) in blood myeloid cells in the CLP vs. sham control mice, as evidenced by a more than 3-fold increase in FLICA (FAM-YVAD-FMK) staining in blood monocytes ($CD115^{+}Ly6G^{-}$) and a 2-fold increase in FLICA staining in neutrophils ($CD115^{-}Ly6G^{+}$), respectively (**Figure 1F-1I)**. These data suggest sustained inflammasome activation at 30 h post-CLP-induced polymicrobial infection. Interestingly, DCA treatment significantly lowered plasma IL-1β (**Figure 1B**) and reduced caspase-1 cleavage in both blood monocytes and neutrophils (**Figures 1F-1I**). Because IL-1β drives neutrophils recruitment and DCA lowered plasma IL-1β, not surprisingly, DCA treatment prevented polymicrobial infection-induced neutrophilia, but not monocytosis (**Figures 1C-1E**). Collectively, our data suggest that inhibition of PDHK attenuates sepsis-induced inflammasome activation *in vivo*, likely contributing to the reduced septic mortality in DCA-treated mice.

PDHK inhibition lowers macrophage NLRP3 inflammasome activation and cell death

As macrophages are one of the primary innate immune cells that can sense a wide range of NLRP3 inflammasome stimuli to mount a robust NLRP3 inflammasome response in our body, we then switched to *in vitro* murine bone marrow-derived macrophages (BMDMs) from wild type (WT) C57/BL6 mice to examine the effect of PDHK inhibition on NLRP3 inflammasome activity and its underlying molecular mechanisms. To induce NLRP3 inflammasome activation, we treated LPS-primed BMDMs with three classical NLRP3 inflammasome activators: a) ATP, which activates P2X7 receptors, inducing K^{+} efflux; b) nigericin, which forms pores on the plasma membrane, leading to K^{+} efflux; and c) monosodium urate crystals (MSU), which induces lysosomal rupture following phagocytosis, as depicted in **Figure 2A**. To examine the effect of PDHK inhibition on inflammasome activation in BMDMs, we utilized two PDHK pharmacological inhibitors: DCA and JX06. Pan-PDHK inhibitor DCA blocks the four PDHK isoforms by binding to the pyruvate binding pocket on the kinase, while JX06 preferentially blocks PDHK1 by forming a disulfide bond with Cys240 in the ATP pocket of PDHK1

(Sun et al., 2015). Briefly, we treated macrophages with DCA or JX06 for 30 min before LPS priming or after LPS priming by adding the inhibitors together with NLRP3 inflammasome inducers. We found that DCA (20 mM) or JX06 (10 μM) significantly reduced ATP, nigericin, or MSU-induced IL-1β secretion regardless of being added before or after LPS priming, except that DCA inhibited MSU-induced IL-1β secretion only when added after the LPS priming step (**Figures 2B-2C**). Interestingly, we observed a more profound effect of DCA or JX06 on IL-1β secretion when adding the inhibitors after LPS priming (**Figures 2B-2C**). Therefore, in most subsequent experiments described in this study, DCA or JX06 were added to the culture media after LPS priming unless specifically indicated. Additionally, we used ATP as an NLRP3 inflammasome inducer to study the effect and mechanism of PDHK inhibition on inflammasome activation in most experiments.

Next, we examined the dose-effect of DCA or JX06 on IL-1β secretion and caspase-1 cleavage in LPS-primed macrophages in response to ATP-induced inflammasome stimulation. DCA (5-30 mM) or JX06 (5-40 μM) suppressed IL-1β secretion (**Figures 2D** and **2E**) and IL-1β cleavage (IL-1β p17) (**Figures 2F** and **2G**) in the culture supernatant in a dose-dependent manner, as measured by ELISA or immunoblotting, respectively. Moreover, DCA or JX06 dose-dependently suppressed caspase-1 cleavage (caspase-1 p20) in the culture supernatant but did not affect the intracellular protein level of inflammasome components, such as pro-IL-1β, pro-caspase-1, NLRP3, or ASC (**Figures 2F** and **2G**). These data suggest that DCA or JX06-mediated NLRP3 inflammasome inactivation mainly occurs at the inflammasome complex assembly step (Signal 2) but not the LPS priming step (Signal 1). To confirm this, we next assessed the transcript expression of pro-IL-1β or NLRP3 in LPS-primed macrophages treated with or without PDHK inhibitors. As expected, LPS priming significantly up-regulated IL-1β and NLRP3 expression at the transcript level, compared to the vehicle control or inhibitor-only groups (**Figures 2H** and **2I**). However, DCA (20 mM) or JX06 (10 μM) showed a minor to no effect on the transcript expression of pro-IL-1β or NLRP3 when added before or after LPS priming (**Figures 2H** and **2I**). Consistently, we observed that DCA and JX06 induced a significant reduction in caspase-1 cleavage in macrophages in response to LPS plus nigericin (**Figures S1A-S1B**) or MSU (**Figures S1C-S1D**), respectively. Collectively, our results suggest that pharmacological inhibition of PDHK blocks macrophage NLRP3 inflammasome activation primarily by attenuating caspase-1 cleavage (Signal 2).

Aside from its role in cleaving pro-IL-1β, caspase-1 also cleaves and activates gasdermin D (GSDMD), which forms pores in the plasma membrane, causing cell swelling (ballooning effect) and death, known as pyroptosis (Shi et al., 2015, Chen et al., 2016, Kayagaki et al., 2015). Therefore, we next examined macrophage morphological changes and cell death in the inflammasome-activated macrophages treated with or without PDHK inhibitors. We found that PDHK inhibition protected macrophages against inflammasome-induced cell death, as shown by decreased propidium iodide (PI) or 7-amino-actinomycin D (7-AAD) staining (**Figures 2J** and **2K**), likely resulting from attenuated caspase-1 cleavage in those macrophages. Further, PDHK inhibition

prevented NLRP3 induced cellular swelling as indicated by decreased cellular area in DCA- or JX06-treated vs. LPS plus ATP-treated macrophages (**Figures S1E** and **S1F**).

Taken together, our results suggest that PDHK inhibition protects macrophages against NLRP3 inflammasome activation-mediated inflammation and cell death. Furthermore, because DCA and JX06 displayed similar inhibitory effects on NLRP3 inflammasome activation, our results suggest that PDHK inhibition per se, rather than the particular molecular site of inhibition on the kinase, is the critical factor accounting for inflammasome inhibition.

PDHK inhibition reprograms cellular metabolism in NLRP3 inflammasome-activated macrophages

PDHK is a known metabolic regulator that controls the activity of the gate-keeping enzyme complex PDC (Patel et al., 2014, Klyuyeva et al., 2019, Karpova et al., 2003, Stacpoole, 2012), and metabolic reprogramming of macrophages regulates both LPS priming and the NLRP3 inflammasome complex assembly (Meyers and Zhu, 2020). We next assessed metabolic changes that occur with or without PDHK inhibition following NLRP3 inflammasome activation. To do this, we performed high-resolution metabolomics analysis of cellular metabolites in control and LPS plus ATP-stimulated BMDMs with or without JX06 addition after LPS priming (i.e., at the Signal 2 step). A principal component analysis (PCA) score plot based on metabolite abundance (**Figure 3A**) demonstrated distinct segregation of each treatment group, suggesting different metabolic effects of inflammasome activation in macrophages with or without PDHK inhibition. Among the 236 metabolites detected, 101 metabolites (red) showed significant accumulation in the NLRP3 inflammasome-activated vs. control macrophages (**Figure 3B**). These metabolites included fatty acids (for example, oleic acid, palmitoleate, and linoleic acid), nucleic acids (for example, AMP and IMP), and glycolysis intermediates (for example, 1, 3-bisphosphoglycerate (BPG)/2,3-BPG). The top downregulated metabolites (green, n=93) in the inflammasome-activated vs. control macrophages were antioxidants, including bilirubin, NADH, cysteinyl glycine, and cysteine, suggesting increased oxidative stress in those cells (**Figure 3B**). Metabolite enrichment analysis revealed broad metabolic reprogramming in macrophages upon NLRP3 inflammasome activation, as shown by the top 25 enriched metabolic pathways, including pyruvate metabolism, porphyrin and chlorophyll metabolism, and glutathione metabolism (**Figure 3C**). Inhibition of PDHK by JX06 significantly altered 119 metabolites compared to NLRP3 inflammasome-activated macrophages (**Figure 3D**). Among them, bilirubin was one of the most up-regulated metabolites in JX06-treated macrophages, compared to LPS plus ATP-treated cells, indicating that JX06 prevents bilirubin depletion by inflammasome activation. Also, inhibition of PDHK by JX06 attenuated the accumulation of fatty acids, especially polyunsaturated fatty acids (PUFAs), in inflammasome-activated macrophages (**Figure 3D**). Consistently, the pathway analysis of the metabolites demonstrated that the top regulated metabolic pathways with high pathway impact factors included porphyrin and chlorophyll metabolism, arachidonic acid metabolism, nicotinate and nicotinamide metabolism, citrate cycle (TCA cycle), and pyruvate metabolism (**Figure 3E**). Collectively, these results indicate that PDHK inhibition by JX06 broadly influences

cellular lipid, glucose, redox, and TCA cycle metabolism, demonstrating that PDHK is a vital kinase that controls cellular metabolism under conditions of the NLRP3 inflammasome activation in macrophages.

PDHK inhibition accelerates glycolysis and pentose phosphate pathway (PPP) in NLRP3 inflammasome-activated macrophages

LPS or LPS plus IFN-γ drives macrophages towards aerobic glycolysis (Kelly and O'Neill, 2015), supporting proinflammatory macrophage activation. However, contradictory results regarding the role of glycolysis in NLRP3 inflammasome activation were reported in the literature (Sanman et al., 2016, Wolf et al., 2016, Xie et al., 2016). Nevertheless, as described above, pyruvate metabolism and PPP are two top metabolic pathways altered by JX06 treatment (**Figure 3E**). To better understand the specific pathway changes that occur with PDHK suppression during inflammasome activation, we individually analyzed the abundance of metabolites from these two pathways (**Figure 4A**). We observed a significant increase in 3-phosphoglycerate/2-phosphoglycerate, phosphoenolpyruvate (PEP), pyruvate, and lactate production in LPS+ATP vs. control macrophages (**Figure 4B**), suggesting an enhanced Warburg effect. JX06 treatment elevated glycolytic metabolites beyond that of LPS plus ATP-treated macrophages, except for intracellular lactate (**Figure 4B**), suggesting that PDHK inhibition enhances glycolysis under conditions of inflammasome stimulation. Additionally, inhibition of PDHK also increased the levels of PPP intermediates, including 6-phosphogluconate, sedoheptulose-7-phosphate, and erythrose-4-phosphate (**Figure 4C**), further suggesting that JX06 promotes glucose utilization in the NLRP3 inflammasome-activated macrophages.

To further assess whether PDHK inhibition by JX06 or DCA promotes glycolysis, we next performed a Seahorse glycolysis stress test on LPS-primed macrophages (LPS-activated macrophages), LPS+ATP-treated BMDMs (NLRP3 inflammasome-activated macrophages), and LPS+JX06+ATP or LPS+DCA+ATP (NLRP3 inflammasome-inactivated macrophages). As expected, LPS priming enhanced Warburg glycolysis and glycolysis capacity, as indicated by a significant increase in extracellular acidification rate (ECAR) after injection of glucose and oligomycin, respectively, relative to control cells (**Figures 4D** and **4E**). Interestingly, stimulation of NLRP3 inflammasome by LPS plus ATP significantly lowered glycolysis and glycolysis capacity, as shown by overall decreased ECAR in those cells (**Figures 4D** and **4E**). This result contradicts our metabolomics data, which showed the accumulation of glycolytic intermediates in macrophages following LPS+ATP treatment (**Figure 4B**), a trend typically interpreted as increased glycolytic flux. Despite this discrepancy, DCA and JX06 both increased ECAR and restored glycolysis of inflammasome-activated macrophages to the control level (**Figures 4D** and **4E**). Meanwhile, DCA but not JX06 restored the glycolytic capacity of the LPS+ATP-treated macrophages to the control level. Collectively, our results suggest that PDHK inhibition by DCA or JX06 promotes glycolysis in the NLRP3 inflammasome-activated macrophages.

PDHK inhibition promotes mitochondrial fueling and respiration in NLRP3 inflammasome-activated

macrophages

Given the increased glucose utilization with PDHK inactivation, we next moved to assess whether glucose utilization in the mitochondria increases since pyruvate can be oxidized to form acetyl-CoA to enter into the mitochondrial TCA cycle via PDC (**Figure 4F**). We found that NLRP3 inflammasome activation by LPS+ATP significantly lowered TCA cycle intermediates, including citrate/isocitrate, and cis-aconitate, but increased succinate, relative to untreated control cells (**Figure 4G**). Aside from its entry into the TCA cycle via PDC, pyruvate can also be carboxylated to form oxaloacetate via pyruvate carboxylase (PC), also known as PC-mediated anaplerosis (Jitrapakdee et al., 2008). Oxaloacetate can then yield malate exported to the cytosol, leading to NADPH production through conversion to pyruvate by the cytosolic malic enzyme (malate-pyruvate cycle) (Sugden and Holness, 2011). Oxaloacetate can also be rapidly converted to aspartate, entering into the malate-aspartate shuttle and aspartate-arginino-succinate shunt for generation of cytosolic fumarate and malate (**Figure 4F**). In line with this, we found that concomitant with the changes to TCA cycle intermediates, NLRP3 inflammasome activation significantly lowered the levels of aspartate, suggesting a lower level of oxaloacetate, and lowered alanine, a PC-dependent anaplerotic substrate, suggesting an impaired PC anaplerosis (**Figure 4H**). Additionally, NLRP3 inflammasome activation increased urea cycle intermediates such as ornithine and citrulline (**Figure 4H**). Interestingly, inhibition of PDHK by JX06 elevated the levels of most of the TCA cycle intermediates. Notably, the succinate, malate, and fumarate levels were markedly increased in PDHK-inactivated macrophages (**Figure 4G**), suggesting an increased TCA cycling. In parallel with these changes, PDHK inhibition increased aspartate and alanine, which are PC-dependent anaplerotic products and substrates, respectively, suggesting that PDHK inhibition also promotes PC-mediated anaplerosis. Additionally, JX06 significantly elevated the levels of argininosuccinate, arginine, and citrulline in inflammasome-stimulated macrophages, further suggesting increased activities of pyruvate anaplerosis, in conjunction with enhanced metabolic flux through the malate-aspartate shuttle, aspartate-argininosuccinate shunt, and the urea cycle (**Figure 4H**). These metabolic changes likely favor TCA cycle intermediate replenishment for anabolic energy production.

In addition to mitochondrial fueling through anaplerosis, fatty acids are a crucial source of pyruvate for mitochondria. LPS-induced proinflammatory macrophage activation increases the production of citrate to support fatty acid synthesis, which enhances the priming steps of the NLRP3 inflammasome (Moon et al., 2015b). One interesting finding from our metabolomics analysis is that macrophages reprogramed fatty acid metabolism in response to PDHK inhibition (**Figure 3E**). Of interest, LPS plus ATP-treated macrophages showed increased accumulation of saturated and monounsaturated fatty acids and n-3 and n-6 PUFAs, which were significantly reduced with JX06 treatment (**Figure S2A**). Concomitant with the down-regulation of fatty acids in PDHK-inhibited macrophages, the abundance of carnitine, a known inflammatory reducer (Haghighatdoost et al., 2019), and carnitine metabolites were significantly increased (**Figure S2B**), likely supporting mitochondrial fatty acid oxidation. Collectively, our results indicate that PDHK inhibition promotes mitochondrial fueling through multiple mechanisms under conditions of NLRP3 inflammasome activation.

Next, we conducted the Seahorse mitochondrial stress test to assess whether the increased mitochondrial fueling by PDHK inhibition supports mitochondrial respiration. LPS plus ATP-induced NLRP3 inflammasome activation, but not LPS priming, impaired mitochondrial respiration, as shown by a significant reduction in basal respiration, maximal respiration, and ATP production-linked respiration (**Figures 4I** and **4J**). Not surprisingly, PDHK inhibition by DCA or JX06 markedly improved mitochondrial respiration, as shown by a significantly higher oxygen consumption rate as compared to inflammasome-activated cells (**Figures 4I** and **4J**). Consistent with the changes in ECAR and OCR, NLRP3 inflammasome activation by LPS plus ATP decreased total ATP production in macrophages, as quantified by the Seahorse XF real-time ATP rate assay (**Figure 4K**). Interestingly, PDHK inhibition by DCA rescued inflammasome activation-induced bioenergetic defects by elevating both glycolytic and mitochondrial ATP production (**Figure 4L**). A similar trend was seen in JX06-treated macrophages, although it did not reach statistical significance (**Figure 4L**). Taken together, our results suggest that PDHK supports mitochondrial fueling upon NLRP3 inflammasome activation, restoring mitochondrial metabolic and energy homeostasis.

PDHK-regulated NLRP3 inflammasome inactivation is independent of glucose metabolism

To assess whether the enhanced glucose utilization accounts for PDHK inhibition-mediated NLRP3 inflammasome inactivation, we blocked glycolysis, PPP, and mitochondrial glucose metabolism by adding pharmacological inhibitors 30 min before stimulating macrophages with ATP in the presence or absence of DCA (**Figure 5A**). Blockade of glycolysis using 2-DG (blocking hexose kinase), heptelidic acid (HA, blocking GAPDH), or sodium oxamate (blocking lactate dehydrogenase) at the complex assembly step (Signal 2) failed to alter IL-1β secretion or reverse the inhibitory effects of DCA on IL-1β secretion (**Figure 5B**). Blockade of PPP by dehydroepiandrosterone (DHEA, blocking glucose-6-phosphate dehydrogenase) lowered LPS plus ATP-induced IL-1β secretion but was unable to reverse the effect of DCA on the inflammasome (**Figure 5C**). These data suggest that neither cytosolic glycolysis nor PPP flux is attributable to attenuated IL-1β secretion in PDHK-inhibited macrophages in response to ATP-induced NLRP3 inflammasome activation. Next, blockade of mitochondrial pyruvate carrier (MPC) by UK5099 (**Figure 5D**), PDH-dependent glucose oxidation by CPI-613 (also blocking α-ketogluconate dehydrogenase (α-KGDH) in the TCA cycle) (**Figure 5E**), or inhibition of PC-mediated pyruvate anaplerosis (**Figure 5F**), suppressed ATP-induced IL-1β secretion, respectively, but had no impact on the inhibitory effect of DCA on ATP-induced IL-1β secretion. Additionally, blockade of other metabolic pathways that were up-regulated in PDHK-inhibited macrophages (**Figure S3A**), for example, the malate-aspartate shuttle by aminooxy acetic acid (AOAA) (**Figure S3B**), aspartate-arginino-succinate shunt by fumonisin B1 (**Figure S3C**), or fatty acid oxidation by etomoxir (**Figure S3D**), all failed to reverse the inhibitory effect of DCA on ATP-induced IL-1β secretion. These results suggest that PDHK inhibition-mediated NLRP3 inflammasome inactivation does not directly result from enhanced glucose metabolism or other altered metabolic pathways that are coupled with the TCA cycle.

PDHK-mediated NLRP3 inflammasome inactivation is independent of PDH

Initially, we hypothesized that PDHK inhibition enhances PDC activation, which promotes glucose/pyruvate oxidative metabolism in macrophages, leading to the inactivation of the NLRP3 inflammasome. For this hypothesis to be true, inhibition of PDH should reverse the effect of DCA on NLRP3 inflammasome activation. However, the failure of the glucose metabolism inhibitors to reverse the DCA effect on IL-1β secretion (**Figures 5B-5F**) suggests a PDH-independent mechanism that underlies PDHK inhibition-mediated NLRP3 inflammasome inactivation. To test this, we knocked down PDHe1α, the PDC subunit whose activity is negatively regulated by PDHK-mediated phosphorylation, using PDHe1α-specific siRNA. PDHe1α transcript expression showed a 60% reduction in PDHe1α-silenced macrophages (**Figure 5G**). Silencing PDHe1α did not significantly alter LPS plus ATP-induced IL-1β section (**Figure 5H**), and appeared to increase caspase-1 cleavage (**Figure 5I**). Interestingly, both DCA and JX06 could still efficiently lower LPS plus ATP-induced IL-1β production in PDHe1α-silenced macrophages (**Figure 5H**). These data imply that a) inhibition of PDH is unable to reverse the effect of PDHK inhibition on NLRP3 inflammasome activity; b) PDHK inhibition-mediated NLRP3 inflammasome inactivation is not caused by PDH-induced glucose oxidation.

Next, we knocked down the gene expression of the predominant macrophage PDHK isoforms to assess whether genetic inhibition of PDHK could mimic the effect of pharmacological inhibitors on NLRP3 inflammasome activity. PDHK1 showed the highest expression in macrophages among the four isoforms, whereas PDHK4 was the lowest abundant isoform at the transcript level (**Figure 5J**). NLRP3 inflammasome stimulation by LPS plus ATP lowered the transcriptional expression of PDHK isoforms 1 and 2, but not 3 or 4 (**Figure 5J**). Based on these results, we silenced the predominant macrophage PDHK isoforms 1 and 2. PDHK isoform-specific siRNAs effectively knocked down each isoform in macrophages (**Figure 5K**) and lowered LPS plus ATP-induced IL-1β secretion (**Figure 5L**). Moreover, silencing PDHK isoform 1, and to a much lesser extent, silencing isoforms 2, reduced LPS plus ATP-induced caspase-1 cleavage (**Figure 5M**). These data suggest that similar to PDHK pharmacological inhibitors, genetic inhibition of PDHK also suppresses NLRP3 inflammasome activation. Collectively, our results indicate that PDHK activity regulates NLRP3 inflammasome activity in macrophages, independent of PDC-dependent glucose oxidation.

PDHK inhibition promotes autophagic flux in NLRP3 inflammasome-activated macrophages

Because our data suggest that metabolism is not the driver of PDHK regulated dampening of NLRP3 inflammasome activity, we next looked to other cellular processes that could be responsible. Autophagy is a cellular process for organelle and protein turnover. Notably, autophagy dampens NLRP3 inflammasome activation via multiple mechanisms, including clearance of assembled inflammasome complexes and removal of secondary stimuli that could initiate complex assembly (Kim et al., 2016, Deretic, 2021). On the other hand, autophagy facilitates IL-1β secretion via an unconventional secretory pathway (Dupont et al., 2011). Therefore,

we next asked whether 1) PDHK inhibition can promote autophagic flux in NLRP3 inflammasome-activated macrophages, and if true, 2) whether autophagy is responsible for the NLRP3 inflammasome inactivation in PDHK inhibited macrophages. To examine autophagic flux, we treated LPS-primed macrophages with ATP in the absence or presence of bafilomycin (blocking autophagosomal degradation in lysosomes) with or without DCA or JX06 over a 2 h time course. In the absence of bafilomycin, autophagy-associated protein LC3-II showed less expression in PDHK-inhibited macrophages compared to LPS plus ATP-treated cells. In contrast, in bafilomycin-treated macrophages, DCA or JX06 treatment enhanced the accumulation of both LC3-I and LC3-II (**Figure 6A**). These data suggest that PDHK inhibition promotes autophagic flux under conditions of NLRP3 inflammasome activation. Additionally, we observed increased expression of autophagic adaptor protein p62, which facilitates chaperon-mediated autophagy, of mitochondrial Tu translation elongation factor (TUFM), which promotes mitophagy (autophagy of mitochondria) by interacting with Atg5-Atg12, Atg16L1 (Lei et al., 2012), or PINK1 (Lin et al., 2020) , and of Parkin, which mediates mitophagy in a VDCA1 and p62-dependent manner (Geisler et al., 2010), in DCA or JX06-treated macrophages (**Figure 6B**), suggesting that PDHK inhibition promotes autophagic and mitophagic activities in inflammasome-activated macrophages. Because AMP kinase (AMPK) serves as an upstream regulator of autophagy and DCA has been shown to activate AMPK in cardiac tissues (Li et al., 2019), we next examined the effect of PDHK inhibition on AMPK signaling in NLRP3 inflammasome activated macrophages. Consistent with the published work (Li et al., 2019), DCA, and to a lesser extent, JX06, activated the AMPK signaling pathway, as shown by increased p-AMPK and its downstream signaling molecule p-acetyl-CoA carboxylase (ACC), in a time-dependent manner (**Figure 6C**), suggesting that enhanced autophagy/mitophagy in PDHK-inhibited macrophages may at least partially result from increased AMPK signaling.

We then asked whether the enhanced autophagy/mitophagy can account for the attenuated NLRP3 inflammasome activation in PDHK-inhibited macrophages. We first used genetic autophagy-deficient BMDMs from myeloid-specific atg5$^{-/-}$ mice to address this question. The atg5-deficient macrophages displayed a 95% reduction in atg5 expression at the transcript level relative to control cells (**Figure 6D**). Atg5$^{-/-}$ macrophages showed significantly less IL-1β secretion than control (**Figure 6E**), likely due to defective unconventional IL-1β secretion. Interestingly, DCA and JX06 maintained their capacity to reduce IL-1β secretion (**Figure 6E**) and caspase-1 cleavage (**Figure 6E**) in atg5$^{-/-}$ macrophages. Similar results were obtained with 3-methyladenine (3-MA) to block autophagy (**Figure 6G**). Together, our data suggest that PDHK inhibition promotes autophagy/mitphagy activation under conditions of NLRP3 inflammasome activation. However, autophagy is not required for decreased NLRP3 inflammasome activity in PDHK-inhibited macrophages.

PDHK inhibition protects against NLRP3 inflammasome-induced mitochondrial stress

Since mitochondria play a central role in the NLRP3 inflammasome, and mitochondrial oxidative stress supports NLRP3 inflammasome activation (Zhou et al., 2011, Misawa et al., 2013, Nakahira et al., 2011, Zhong et al.,

2018), we next moved to assess whether mitochondria were the mechanism through which PDHK inhibition regulates the activity of the NLRP3 inflammasome. To do so, we first quantified mitochondrial ROS (mtROS) production by staining macrophages with MitoSOX. As expected, activation of the NLRP3 inflammasome by LPS plus ATP triggered mitochondrial oxidative stress in macrophages, as evidenced by a robust mtROS production in those macrophages compared to control (**Figure 7A**). PDHK inhibition by DCA or JX06 counteracted LPS plus ATP-induced mitochondrial oxidative stress, as demonstrated by a 50% reduction in mtROS production (**Figure 7A**). Consistent with this, LPS plus ATP-induced NLRP3 inflammasome activation depleted the metabolites in the methionine-cysteine-glutathione pathways (**Figure S4A**), NAD^+, NADH, $NADP^+$, and other NAD^+ biosynthetic metabolites (**Figure S4B**), reflecting an excessive oxidative stress condition, which was partially restored by JX06 treatment (**Figure S4B**). Together, our data suggest that PDHK inhibition protects macrophages against oxidative stress, particularly mitochondrial oxidative stress. In combination with data demonstrating improved mitochondrial respiration and ATP production in PDHK-inhibited macrophages (**Figure 4**), our results suggest that inhibition of PDHK repurposes mitochondria from ROS production to ATP generation.

To understand how PDHK inhibitors remodel mitochondria in the context of NLRP3 inflammasome activation, we next imaged mitochondria in macrophages stained with MitoTracker Deep Red FM using confocal microscopy. We also analyzed mitochondrial ultrastructure using transmission electron microscopy (TEM). First, as reported (Misawa et al., 2013, Misawa et al., 2015), in response to NLRP3 inflammasome stimulation, mitochondria underwent a morphological change from a string-like shape to a dot-like shape (**Figure 7B**), indicating enhanced mitochondrial fragmentation. Notably, PDHK inhibition by DCA or JX06 maintained mitochondria in a more string-like shape in inflammasome-stimulated macrophages (**Figure 7B**), suggesting that inhibition of PDHK protects against NLRP3 inflammasome-induced mitochondrial damage. Consistent with confocal microscopy analysis, morphometric analysis of TEM images (**Figure 7E**) revealed a significant reduction in both mitochondrial length and perimeter in LPS plus ATP-treated vs. control macrophages (**Figures 7D** and **7E**), suggesting increased mitochondrial fragmentation. Mitochondrial fragmentation was partially abolished by PDHK inhibition, given the fact that DCA or JX06-treated macrophages displayed greater mitochondrial length and perimeter (**Figures 7D** and **7E**). However, PDHK inhibition did not alter the mitochondrial number, aspect ratio (major axis/minor axis), or roundness compared to NLRP3 inflammasome activation (**Figure S4C**). Moreover, NLRP3 inflammasome activation by LPS plus ATP reduced cristae number per mitochondrion (**Figures 7F** and **7G**) and increased cristae widening, as shown by greater cristae maximal width (**Figures 7F** and **7H)**. Interestingly, PDHK inhibition partially restored cristae density and narrowed cristae width compared to LPS plus ATP stimulation (**Figures 7F-7H**). Because cristae shape governs mitochondrial respiration and stacking cristae supports mitochondrial bioenergetics (Cogliati et al., 2013), our data indicate that inhibition of PDHK improves mitochondrial functionality and repurposes mitochondria toward oxidative respiration by preserving mitochondrial morphology and cristae ultrastructure.

PDHK inhibition preserves mitochondrial cristae ultrastructure and inactivates NLRP3 inflammasome partially by up-regulation of mitochondrial OPA1

Mitochondria are dynamic organelles undergoing continual fusion and fission, a process regulated by a family of dynamin-related GTPases. Among them, cytosolic dynamin-related protein 1 (Drp1) mediates mitochondrial fission after recruitment to mitochondria upon phosphorylation on Ser616 and dephosphorylation on Ser637 (Cereghetti et al., 2008, Smirnova et al., 2001). In contrast, mitochondrial fusion proteins mitofusin 1 and 2 (Schrepfer and Scorrano, 2016) and optic atrophy protein 1 (OPA1) (Mishra et al., 2014) control outer mitochondrial membrane (OMM) and inner mitochondrial membrane (IMM) fusion, respectively. Given that decreased mitochondrial fusion and increased mitochondrial fission can cause mitochondrial fragmentation, we next examined the expression of phospho-Drp1 (Ser616) and OPA1 in macrophages. Consistent with the increased mitochondrial fragmentation, the protein level of p-Drp1 (Ser616) was markedly increased at 30 min post ATP treatment and its level reduced to the baseline at 60 or 120 min ATP treatment (**Figure 7I**). OPA1 level remained low during 60 min ATP exposure and slightly increased at 120 min ATP stimulation (**Figure 7I**). Interestingly, PDHK inhibition by DCA attenuated ATP-induced phospho-Drp1 (Ser616) expression and increased OPA1 protein level (**Figure 7I**), suggesting decreased mitochondrial fission and increased mitochondrial fusion. Notably, genetic deletion of PDHK1 also increased OPA1 expression at the basal state and after LPS plus ATP stimulation (**Figure 7J**). OPA1 regulates not only mitochondrial fusion but also cristae remodeling, mitochondrial respiration, and ROS production (Quintana-Cabrera et al., 2018, Mishra et al., 2014, Jang and Javadov, 2020). We next examined if the increased OPA1 is attributable to the attenuated NLRP3 inflammasome activity in PDHK-inhibited macrophages. Interestingly, inhibition of OPA1 by MYLS22, a selective OPA1 inhibitor, partially abolished the suppressive effect of DCA on IL-1β secretion (**Figure 7K)**. Together, our data suggest that PDHK inhibition protects against mitochondrial fragmentation and preserves cristae shape and ultrastructure. Further, PDHK inhibition requires OPA1 to attenuate the activity of the NLRP3 inflammasome.

Discussion

Macrophage NLRP3 inflammasome has emerged as a crucial driver of sepsis-associated inflammation (Danielski et al., 2020). PDHK is a mitochondrial metabolic regulator that dictates the activity of the PDC. By phosphorylating the PDHe1α subunit of PDC, PDHK effectively blocks the conversion of pyruvate into acetyl-CoA such that pyruvate is no longer able to be utilized by the mitochondria in the TCA cycle. Pharmacologically targeting PDHK with pan-PDHK inhibitor DCA enhances septic mouse survival (McCall et al., 2018), rebalances metabolic dysregulation in septic mouse liver (Mainali et al., 2021), or inflammatory THP1 monocytes (Zhu et al., 2020). Here, our *in vivo* study demonstrates that DCA lowers circulating IL-1β concentration, attenuates blood neutrophilia, and reduces caspase-1 activities in blood monocytes and neutrophils in septic mice, suggesting that PDHK promotes NLRP3 inflammasome activation during sepsis. Our *in vitro* study confirms the role of mitochondrial PDHK in supporting NLRP3 inflammasome activation, which appears to be independent of PDH-dependent pyruvate oxidation. Mechanistically, PDHK promotes DRP1-dependent mitochondrial fission and impairs OPA1-dependent mitochondrial fusion and cristae integrity, favoring mitochondrial ROS production over energy generation to support NLRP3 inflammasome-induced inflammation and cell death.

We initially hypothesized that PDHK supports NLRP3 inflammasome activation by down-regulating PDH-dependent pyruvate oxidation or utilization. If this hypothesis were true, inhibition of PDH or mitochondrial pyruvate utilization would counteract the DCA effect on inflammasome activation. Interestingly, blockade of pyruvate entry into mitochondria, inhibition of PC-dependent pyruvate anaplerosis, or inhibition of PDH-dependent pyruvate oxidation by CPI-613 (also inhibiting α-KGDH) at the Signal 2 step all markedly reduced IL-1β secretion. These data suggest that mitochondrial pyruvate metabolism is necessary for NLRP3 inflammasome activation. Consistent with our results, mitochondrial pyruvate-derived citrate can be transported into the cytosol for fatty acid synthesis to support the NLRP3 inflammasome activation (Moon et al., 2015b). PDH-dependent pyruvate flux also enhances LPS-induced macrophage inflammation (Meiser et al., 2016). Importantly, inhibition of mitochondrial pyruvate metabolism could not reverse the suppressive effect of DCA on inflammasome activation. This data suggests that the PDHK-mediated NLRP3 inflammasome activation is an inflammatory pathway distinct from mitochondrial pyruvate metabolism. Further, DCA or JX06 can effectively lower IL-1β secretion in PDHe1α-silenced macrophages. Thus, our findings suggest a novel role for PDHK in regulating the NLRP3 inflammasome, independent of phosphorylation of PDH for pyruvate oxidation.

Mitochondria have long been known to play a central role in NLRP3 inflammasome activation (Zhou et al., 2011). These organelles serve as a source of NLRP3 inflammasome stimuli, including mtROS (Zhou et al., 2011, Cruz et al., 2007), mtDNA (Nakahira et al., 2011, Shimada et al., 2012), and cardiolipin (Iyer et al., 2013). The mitochondria-associated adaptor molecule, MAVS, also acts as the docking site for the NLRP3 inflammasome complex assembly in the cytoplasm (Subramanian et al., 2013). In our study, inhibition of PDHK protected against LPS plus ATP-induced mitochondrial oxidative damage and dysfunction, as evidenced by 1) reduced

mitochondrial fragmentation, 2) preserved cristae ultrastructure, 3) attenuated mitochondrial ROS production, and 4) enhanced mitochondrial ATP generation when comparing PDHK-inhibited macrophages vs. inflammasome activated cells. Notably, mitochondrial cristae shape regulates respiratory chain super-complex stability and assembly (Cogliati et al., 2013). In addition to regulating mitochondrial inner membrane fusion [65], mitochondrial fusion protein OPA1 also directly reshapes cristae and fosters ATP synthase oligomerization and reversal (i.e., ATP hydrolase) activity to support mitochondrial respiration (Quintana-Cabrera et al., 2018). In parallel with the improved mitochondrial morphology and cristae ultrastructure, PDHK-inhibited macrophages displayed decreased mitochondrial fission protein p-DRP1 and conversely increased OPA1 expression. In line with the critical role of OPA1 in maintaining mitochondrial morphology and function, our data further showed that inhibition of OPA1 partially reversed the inhibitory effect of DCA on NLRP3 inflammasome activation. Collectively, our findings highlight a new role for PDHK in supporting mitochondrial oxidative stress/damage, mitochondrial fission over fusion, and cristae remodeling in an OPA1-dependent manner upon NLRP3 inflammasome stimulation.

We propose that PDHK suppresses OPA1 expression and enhances DRP1 phosphorylation by unknown mechanisms to support mitochondrial oxidative stress under conditions of inflammasome activation. It has been reported that PDHK4 can directly phosphorylate SMAD1/5/8 via direct interaction to enhance bone morphogenetic protein 2 (BMP2) signaling and vascular calcification in vascular smooth muscle cells (Lee et al., 2015). Another study reported that PDHK4 sequesters NF-κB/p65 in the cytoplasm under normal conditions via a direct protein-protein interaction in hepatocytes (Wu et al., 2018). Disruption of PDHK4 and p65 association promotes p65 nuclear translocation to activate TNF-induced apoptotic pathway (Wu et al., 2018). These studies indicate that PDHK4 has a dual location and function in mitochondria and cytoplasm. Our study showed that PDHK1 is the most abundant isoform expressed in macrophages, and we found that inhibition of PDHK by DCA or genetic deletion of PDHK1 up-regulated OPA1 expression at baseline and after inflammasome activation. Given that PDHK and OPA1 co-exist in the mitochondrial matrix, we reason that likely, PDHK can regulate OPA1 expression via direct or indirect protein-protein interaction. Moreover, similar to PDHK4, PDHK1 may also translocate to the cytoplasm to regulate p-DRP1 expression under inflammatory conditions. Future studies will be conducted to test these concepts. Approaches such as phosphoproteomics analysis of subcellular compartments likely will provide mechanistic insights into PDHK-regulated inflammasome activation.

At the later stage of sepsis, leukocytes display a generalized metabolic defect at the level of both glycolysis and oxidative metabolism in human septic patients (Cheng et al., 2016). Interestingly, our Seahorse assays showed that LPS plus ATP-induced NLRP3 inflammasome activation rapidly induced metabolic defects. The inflammasome-activated macrophages displayed decreased glycolysis, lower mitochondrial respiration, and reduced ATP production, mimicking the metabolic paralysis at the late stage of sepsis. In contrast, LPS-primed macrophage showed elevated Warburg glycolysis, unaltered mitochondrial respiration, and increased glycolysis

ATP, mimicking the initial phase of sepsis (Cheng et al., 2016). Our data suggest that in response to NLRP3 inflammasome stimulation, macrophages rapidly shift from Warburg glycolysis to metabolic paralysis. Intriguingly, PDHK inhibition at the Signal 2 step can restore both anabolic and catabolic metabolism, as shown by increased glycolysis, enhanced mitochondrial respiration, and improved ATP production in DCA- or JX06-treated macrophages. Consistent with the Seahorse results, our metabolomics analysis demonstrated that inhibition of PDHK by JX06 at the Signal 2 step broadly rewired cellular metabolic pathways, including fatty acid metabolism, pyruvate metabolism, and the TCA cycle. One interesting observation is that PDHK inhibition appears to enhance pyruvate oxidation and anaplerosis to promote pyruvate utilization. Others have reported that pyruvate carboxylation by PC can support TCA cycle function and redox capacity via replenishing TCA cycle intermediates in hepatocytes (Cappel et al., 2019). We reason that very likely, the enhanced pyruvate oxidation and anaplerosis reflects the improved mitochondrial function in PDHK-inhibited macrophages. Moreover, fused mitochondria are required by free fatty acids to distribute in mitochondria for maximal oxidation in starved cells (Rambold et al., 2015). Indeed, our metabolomics data showed that PDHK inhibition markedly altered fatty acid metabolism, as evidenced by decreasing free fatty acid accumulation and conversely increasing acyl-carnitines. Together, our results suggest that inhibition of PDHK promotes mitochondrial fusion, which maximizes fuel utilization to support energy production.

An unusual set of data worth discussing was the defective glycolysis in NLRP3 inflammasome-activated macrophages observed from our Seahorse experiment assay but not the metabolomics analysis. The exact causes of this discrepancy are unknown. One possibility is that the metabolomics analysis reflects a snapshot of the steady-state level of intracellular metabolites in macrophages. Therefore, the accumulation of glycolytic intermediates could be interpreted as increased glucose flux or decreased glucose utilization. Another possibility is that LPS plus ATP rapidly shifts macrophage metabolism from hyper-glycolysis (captured by our metabolomics analysis) to hypo-glycolysis (captured by the seahorse assay). Despite the discrepancy, both assays consistently suggest that PDHK inhibition enhances glycolysis and mitochondrial oxidative respiration, increasing overall energy production in macrophages under conditions of NLRP3 inflammasome stimulation.

In another attempt to look into the underlying mechanism of the reduced NLRP3 inflammasome activation, we examined autophagy, a cellular process for organelle and protein turnover. Autophagy inhibits NLRP3 inflammasome activation through multiple mechanisms. For example, autophagy can inhibit mitochondrial DNA release (Nakahira et al., 2011), promote inflammasome complex degradation (Shi et al., 2012, Harris et al., 2011), or clear damaged mitochondria (Zhou et al., 2011). In our hands, autophagy-deficient macrophages by using 3-MA or deletion of atg5 consistently showed lower IL-1β secretion in response to LPS plus ATP stimulation. Interestingly, it is reported that autophagy can facilitate the extracellular delivery of IL-1β through an unconventional secretory pathway (Dupont et al., 2011). Therefore, in the autophagy-deficient macrophages, the level of extracellular IL-1β is the net result of the increased IL-1β cleavage due to enhanced inflammasome

activation and the attenuated IL-1β secretion due to the impaired unconventional secretory pathway. Nonetheless, similar to what has been found in cancer cells (Lin et al., 2014, Gong et al., 2013), our data showed that PDHK inhibition promotes autophagic flux and mitophagy in macrophages in response to NLRP3 inflammasome stimulation. However, autophagy is not responsible for the attenuated NLRP3 inflammasome activation in PDHK-inhibited macrophages, given that DCA or JX06 can still effectively lower IL-1β and caspase-1 cleavage in autophagy-defective macrophages. Despite the indispensable role of autophagy in IL-1β secretion, the enhanced autophagic flux, especially mitophagy, was associated with improved mitochondrial morphology and function in PDHK-inhibited macrophages, suggesting that PDHK inhibition may improve overall mitochondrial homeostasis via mitophagy activation.

In conclusion, our current study highlights that mitochondrial function and metabolism play a central role in macrophage NLRP3 inflammasome activation. Independent of its canonical regulation of pyruvate oxidation, mitochondrial PDHK expression exaggerates mitochondrial damage and oxidative stress to support NLRP3 inflammasome activation at least partially by inhibiting mitochondrial OPA1. Targeting PDHK dampens NLRP3 inflammasome activity in inflamed macrophages *in vitro* and septic mice *in vivo*. In addition to sepsis, PDHK has emerged as a critical target in other disease states, including diabetes [54], cardiovascular diseases [55]. Hence, our study provides evidence for the therapeutic targeting of PDHK to treat inflammatory conditions.

Limitations of the study

In this study, we utilized various pharmacological inhibitors to examine the effect of the metabolic pathways on NLRP3 inflammasome activation. Although those inhibitors are well-characterized in the literature, there is still potential that non-specific untargeted effects exist and interfere with the data interpretation. Secondly, we blocked each targeted pathway using a pathway-specific inhibitor when we examined the impact of metabolic shift-induced by PDHK inhibition on NLRP3 inflammasome activation. We do not rule out that there could be a combinatory effect through multiple pathways on PDHK-mediated NLRP3 inflammatory activation. Lastly, we only tested the role of PDHK in NLRP3 inflammasome activation using murine macrophages and septic mice. Confirming our findings in human cells and sepsis patients will be critical to support the translational relevance of the current study.

Acknowledgments

The authors gratefully acknowledge Ken Grant, Paula Graham, and Debbie Golden of the Cellular Imaging Shared Resource (CISR) of Atrium Health Wake Forest Baptist for technical assistance with confocal and transmission electron microscopy. The authors also would like to acknowledge pilot funding support from the Wake Forest Center for Redox Biology and Medicine (CRBM) and helpful feedback during the CRBM Metabolism and Inflammation working group meetings. Finally, the authors would like to thank the Quinn lab of Wake Forest for their contribution of reagents. This study was supported by NIH R35 GM126922 (CEM), NIH R01 CA248037 (HKL), NIH R01 HL132035 (XZ), NIH T32GM127261 (AKM), and NIH T32 AI007401 (AKM). The study was also supported by the National Center for Advancing Translational Sciences of the National Institutes of Health under Award Number UL1TR001420 (Research Assistant fund to XZ).

Author Contributions

X.Z. conceived the study; A.K.M., Z.W., W.H., Q.Z., and M.Z. conducted the experiments; J.L. conducted the high-resolution metabolomics analysis and edited the manuscript; R.K.M provided advice related to TEM; J.W.L. provided advice related to metabolomics analysis, helped with data discussion, and provided comments; H.K.L., C.M.F., and C.E.M helped with data discussion and provided comments and revisions; Z.W. wrote the methods and edited the manuscript; A.K.M. and X.Z. wrote the manuscript.

Declaration of Interests

The authors declare no competing interests.

Inclusion and diversity statement

One or more of the authors of this paper self-identified as living with a disability.

Figure legends

Figure 1. PDHK inhibition lowers plasma IL-1β and blood monocyte and neutrophil caspase-1 activity in septic mice.

Mice were i.p. injected with 25 mg/kg DCA or saline as vehicle control 24 h post cecal ligation and puncture. Sham-operated mice were used as another control. Blood was collected after 6 h of DCA injection.

(**A**) Schematic of mouse treatments.

(**B**) Plasma IL-1β was measured by ELISA.

(**C-E**) Peripheral blood cells were stained with FAM-YVAD-FMK probe (FLICA), CD115-PE, Ly6C/Ly6G-Percp-Cy5.5, and CD45-APC. Percentage of monocytes ($CD115^+Ly6G^-$) and neutrophils ($CD115^-Ly6G^+$) (D-E) in $CD45^+$ cells were analyzed by flow cytometry.

(**F-G**) Peripheral blood cells were stained with CD115-PE, Ly6C/Ly6G-Percp-Cy5.5, and CD45-APC. The percentage of $FLICA^+$ cells in blood monocytes ($CD45^+CD115^+Ly6G^-$) was analyzed by flow cytometry.

(**H-I**) Peripheral blood cells were stained with FAM-YVAD-FMK probe (FLICA), CD115-PE, Ly6C/Ly6G-Percp-Cy5.5, and CD45-APC. The percentage of $FLICA^+$ cells neutrophils ($CD45^+CD115^-Ly6G^+$) was analyzed by flow cytometry.

Each symbol represents an individual mouse. *P < 0.05; **P < 0.01; ***P < 0.001; ns: non-significant, one-way ANOVA with post hoc Tukey's multiple comparisons test.

Figure 2. PDHK inhibition lowers macrophage NLRP3 inflammasome activation and cell death.

BMDMs were first primed with 300 ng/ml LPS for 3 h, then stimulated with 5mM ATP for 1 h, 10 μM nigericin (NIG) for 1 h, or 0.6 mg/ml monosodium urate crystals (MSU) for 6 h, respectively.

(**A**) Schematic of BMDM treatments and timing

(**B-C**) 20 mM DCA, 10 μM JX06, or DMSO (vehicle control for JX06) were added before or after LPS priming. IL IL-1β concentrations in the culture supernatant were analyzed by ELISA.

(**D-E**) 5-20 mM DCA, 5-40 μM JX06, or DMSO (vehicle control for JX06) were added after LPS priming. IL-1β concentrations in the culture supernatant were analyzed by ELISA.

(**F-G**) 5-20 mM DCA, 5-40 μM JX06, or DMSO (vehicle control for JX06) were added after LPS priming. Protein expression in the culture supernatant (Sup) and whole-cell lysates (Lys) was analyzed by immunoblotting.

(**H-I**) 20 mM DCA or 10 μM JX06 were added before or after LPS priming. mRNA expression of NLRP3 inflammasome components was measured by qPCR.

(**J-K**) Cell death was measured by staining macrophages with 7-AAD or PI and analyzed by flow cytometry. Groups with different letters are significantly different (p<0.05), one-way ANOVA with post hoc Tukey's multiple comparisons test.

Figure 3. PDHK inhibition rewires macrophage metabolism.

The high-resolution metabolomics data were collected using 300 ng/ml LPS-primed BMDMs treated with 5 mM ATP plus 10 uM JX06 or DMSO as vehicle control for 45 min. The analysis was performed using MetaboAnalyst 5.0.

(**A**) Principal component analysis of the metabolites in BMDMs using MetaboAnalyst 5.0.

(**B**) Volcano plot of the metabolites in LPS+ATP vs. control macrophages, plotted using Graphpad 7.0.

(**C**) The top 25 enriched metabolic pathways in LPS+ATP treated vs. control BMDMs, identified by enrichment analysis and ranked according to p values.

(**D**) Volcano plot of the metabolites in JX06 vs. LPS+ATP treated macrophages, plotted using Graphpad 7.0

(**E**) The top 10 metabolic pathways were altered by JX06 treatment, identified by the pathway analysis and ranked according to p values.

Figure 4. PDHK inhibition accelerates glycolysis, PPP, and TCA cycling.

(**A**) Diagram of glycolysis and pentose phosphate pathway (PPP).

(**B**) Heatmap of the intermediates in the glycolysis pathway from the high-resolution metabolomics analysis.

(**C**) Heatmap of the intermediates in PPP from the metabolomics analysis.

(**D-E**) Seahorse analysis of extracellular acidification rates (ECAR) in BMDMs treated with LPS (300 ng/ml), LPS (300 ng/ml) + ATP (5 mM) in the presence or absence of DCA (20 mM) or JX06 (10 uM) for 1 h.

(**F**) Diagram of TCA cycle, pyruvate carboxylase (PC)-mediated anaplerosis, malate-aspartate shuttle, aspartate-argininosuccinate shunt, and the urea cycle.

(**G**) Heatmap of the intermediates in the TCA cycle.

(**H**) Heatmap of the intermediates in the PC-mediated anaplerosis pathway, aspartate-argininosuccinate shunt, and urea cycle.

(**I-J**) Seahorse analysis of oxygen consumption rates (OCR) in BMDMs treated with LPS (300 ng/ml), LPS (300 ng/ml) + ATP (5 mM) in the presence or absence of DCA (20 mM) or JX06 (10 uM) for 1 h.

(**K-L**) Seahorse XF real-time ATP rate analysis of BMDMs. Glycolytic ATP and mitochondrial ATP production rate were calculated.

Groups with different letters are significantly different ($p<0.05$). $^{\#}$: $p<0.05$, between LPS+ATP and control groups; *: $p<0.05$, between LPS+ATP and LPS+JX06+ATP groups; one-way ANOVA with post hoc Tukey's multiple comparisons test.

Figure 5. PDHK-mediated NLRP3 inflammasome activation is independent of glucose metabolism or pyruvate dehydrogenase.

BMDMs or thioglycollate-elicited peritoneal macrophages (PMs) were stimulated with LPS (300 ng/ml) for 3 h and ATP for 1 h to induce the NLRP3 inflammasome activation. DCA (20 mM) or JX06 (10 μM) were added after LPS priming.

(**A**) The targeting sites of the pharmacological inhibitors are indicated.

(**B-F**) IL-1β secretion from LPS plus ATP-treated BMDMs. Hexokinase inhibitor 2-deoxy-D-glucose (2-DG; 10 mM), glyceraldehyde-3-phosphate dehydrogenase (GAPDH) inhibitor heptelidic acid (HA, 15 μM), lactate dehydrogenase inhibitor sodium oxamate (40 mM), glucose-6-phosphate dehydrogenase (G6PD) inhibitor dehydroepiandrosterone (DHEA) (200 μM), mitochondrial pyruvate carrier (MPC) inhibitor UK5099 (5 μM), pyruvate carboxylase (PC) inhibitor chlorothricin (100 μM), or pyruvate dehydrogenase (PDH) and α-ketoglutarate dehydrogenase (KGDH) inhibitor CPI-613 (200 μM), were added 30 min before ATP.

(**G**) Pdhe1a mRNA expression in control and PDHe1a siRNA transfected elicited PMs.

(**H-I**) IL-1β secretion (H) and caspase-1 cleavage (I) in the culture supernatant from control siRNA and Pdhe1a siRNA transfected elicited PMs treated with or without LPS plus ATP in the presence or absence of DCA or JX06.

(**J**) mRNA expression of PDHK isoforms in BMDMs treated with or without LPS plus ATP. Gene expression was normalized to PDHK1 expression in unstimulated macrophages.

(**K**) Transcript expression of PDHK isoform 1, 2, or 4 in control and isoform-specific siRNA transfected elicited PMs, respectively.

(**L-M**) IL-1β secretion (L) and caspase-1 cleavage (M) in the culture supernatant from control siRNA and isoform-specific siRNA transfected elicited PMs treated with or without LPS plus ATP.

Groups with different letters are significantly different ($p<0.05$); *$P < 0.05$; **$P < 0.01$; ***$P < 0.001$; ****$P < 0.0001$; ns: non-significant. One-way ANOVA with post hoc Tukey's multiple comparisons test (Figures 5B-5F, 5H, 5L); unpaired, two-tailed student's T-test (Figures 5G, 5J, and 5K).

Figure 6. Autophagy is unnecessary for down-regulation of the NLRP3 inflammasome by PDHK inhibitors.

(**A**) BMDMs were primed with 300 ng/ml LPS for 3 h, followed by 5 mM ATP in the presence or absence of 20 mm DCA or 10 uM JX06 for 0-120 min. Immunoblotting analysis of LC3 expression in BMDMs. 50 nM bafilomycin A1 was added together with ATP to monitor the autophagic flux.

(**B**) Immunoblotting analysis of P62 and mitochondrial Tu translation elongation factor (TUFM) expression in BMDMs as described in (**A**) except for bafilomycin A1 treatment.

(**C**) Immunoblotting analysis of p-AMPK and p-ACC expression in BMDMs as described in (**A**) except for bafilomycin A1 treatment.

(**D**) Atg5 mRNA expression in macrophages from WT and macrophage-specific atg5 knockout (KO) mice.

(**E-F**) IL-1β secretion (E) and caspase-1 cleavage (F) in the culture supernatant from WT and Atg5KO BMDMs treated with or without LPS (300 ng/ml) plus ATP (5 mM) in the presence or absence of DCA (20 mM) or JX06 (10 μM).

(G) BMDMs were pre-incubated with 3-methyladenine (3-MA, 5 mM) for 30 min before treated with or without LPS (300 ng/ml) plus ATP (5 mM) in the presence or absence of DCA (20 mM) or JX06 (10 μM). IL-1β concentration in the culture supernatant was measured by ELISA.

*$P < 0.05$; ****$P < 0.0001$; ns: non-significant. One-way ANOVA with post hoc Tukey's multiple comparisons test.

Figure 7. PDHK inhibition protects against NLRP3 inflammasome partially by up-regulation of mitochondrial OPA1.

BMDMs were primed with 300 ng/ml LPS for 3 h, followed by 5 mM ATP in the presence or absence of 20 mM DCA or 10 μM JX06 for 1 h (except in Figure 7H, LPS plus ATP for 2h).

(**A**) Macrophages were stained with MitoSOX (5 μM) and analyzed by flow cytometry.

(**B**) Confocal images of BMDMs stained with MitoTracker Deep Red (red) and DAPI (blue). Scale bar=? nm.

(**C**) Representative transmission electron microscopy (TEM) images of BMDMs. Scale bar=500 nm.

(**D-E**) Mitochondrial length and perimeter were quantified.

(**F**) Representative mitochondrial TEM images. Scale bar=100 nm.

(**G-H**) Mitochondrial cristae number per mitochondrion and cristae width.

(**I**) Immunoblotting analysis of p-Drp1 (ser616) and OPA1 in BMDMs.

(**J**) Immunoblotting analysis of OPA1 in peritoneal macrophages. Macrophages were first transfected with control siRNA and PDHK isoform-specific siRNA before treated with or without LPS plus ATP.

(**K**) IL-1β level in the culture supernatant from LPS plus ATP-treated BMDMs. OPA1 inhibitor MYLS22 (50 μM) was added 30 min before ATP treatment.

(**L**) caspase-1 cleavage in the culture supernatant from LPS plus ATP-treated BMDMs. OPA1 inhibitor MYLS22 (50 μM) was added 30 min before ATP treatment.

Groups with different letters are significantly different ($p<0.05$); One-way ANOVA with post hoc Tukey's multiple comparisons test.

Methods

Mice

C57BL/6 (stock 000664) and LysMcre (stock 004781) mice were purchased from Jackson Laboratories. Atg5$^{flox/flox}$ mice were purchased from Riken BioResource Center (stock RBRC02975). Heterozygous atg5 macrophage-specific knockout (atg5$^{flox/+}$Lyscre^{+}) mice were generated by crossing atg5$^{flox/flox}$ mice and LysMcre mice. Homozygous atg5 macrophage-specific knockout (atg5$^{flox/flox}$LysMcre^{+}) and WT control mice (atg5$^{flox/flox}$) were generated by intercrossing the heterozygous mice, as described previously (Shen et al., 2017). Mice were housed in a pathogen-free facility on a 12 h light/dark cycle and received a standard laboratory diet. Cecal ligation and puncture (CLP) were performed to induce intra-abdominal polymicrobial infection in C57 BL/6 male mice at the age of 12 weeks as described previously (McCall et al., 2018). Sham-operated mice were used as a control. DCA (25 mg/kg) or saline was injected intraperitoneally (i.p.) 24 h post-CLP. Mice were euthanized 30 hours post CLP. All animal experimental protocols were approved by the Wake Forest University Animal Care and Use Committee.

Cell culture and treatment

Bone marrow-derived macrophages (BMDM) and thioglycollate-elicited peritoneal macrophages were cultured as described previously (Zhu et al., 2008, Wang et al., 2020). Briefly, mouse bone marrow was cultured in low glucose DMEM supplemented with 30% L929 cell-conditioned medium, 20% FBS, 2 mM L-glutamine, 1 mM sodium pyruvate, 100 U/ml penicillin, and 100 µg/ml streptomycin for 6-7 days until the cells reached confluence. BMDMs were then reseeded in culture dishes overnight in RPMI-1640 medium containing 1% Nutridoma-SP medium (Sigma-Aldrich) before any treatment. Thioglycollate-elicited peritoneal macrophages were harvested from mice by washing peritoneal cavities using cold PBS 3 days after i.p. injection of 1 ml of 10% thioglycollate (Sigma-Aldrich). After a 2 h Incubation in RPMI-1640 media containing 10% FBS, 100 U/ml penicillin, and 100 µg/ml streptomycin, floating cells were removed, and adherent macrophages were used for experiments. To induce NLRP3 inflammasome activation, macrophages were first primed with 300 ng/ml LPS (E. coli 0111; B4, Sigma-Aldrich) before stimulated with 5 mM ATP (Sigma-Aldrich) for 15 min to 120 min, 10 µM nigericin (InvivoGen) for 1 h, 0.6 mg/ml monosodium urate crystals (MSU) (InvivoGen) for 6 h, as indicated in the figure legends. To inhibit PDHK, macrophages were pretreated for 30 min before LPS priming or after LPS priming (together with the NLPR3 inflammasome stimuli as described above) with DCA (5-30 mM, Sigma-Aldrich), JX06 (5-40 µM, Rocris) for an indicated time as described in the figure legend. In some experiments, LPS-primed macrophages were treated with 2-DG (10 mM, Sigma-Aldrich), heptelidic acid (15 µM, Cayman Chemical), sodium oxamate (40 mM, Santa Cruz Biotechnology), DHEA (200 µM, EMD Millipore), UK5099 (5 µM, Cayman Chemical), CPI-613 (200 µM, Cayman Chemical), chlorothricin (100 µM, Cayman Chemical), AOAA (1 mM, Cayman Chemical), fumonisin B1 (15 µM, Cayman Chemical), MYLS22 (50 µM, MedChemExpress), ML385 (5 µM, MedChemExpress), etomoxir (50 µM, Cayman Chemical), bafilomycin A1 (50 nM, In vivoGen), or 3-MA (5

mM, Sigma-Aldrich), as indicated in the figure legends. PBS, DMSO, or ethanol was used as vehicle control in the inhibitor experiments.

Flow cytometry

After removing the red blood cells using ACK lysing buffer (Gibco), peripheral white blood cells were stained with FLICA 660-YVAD-FMK (1:150 dilution, ImmunoChemistry Technologies), CD115-PE (eBioscience, no. 12-1152), Gr1(Ly6C/G)-PerCP-Cy5.5 (BioLegend, no. 108427), and CD45-APC (BD Pharmingen, no. 559864). Data were acquired on a BD FACS Canto II instrument (BD Biosciences) and analyzed using FlowJo analytical software (version 7.6.5, TreeStar). BMDMs were stained with 7-AAD (Invitrogen, cat# V35123) or PI (Invitrogen, Cat# P3566) according to the manufacturer's instructions. Data were acquired on a BD FACSCalibur and analyzed using FlowJo analytical software (version 7.6.5, TreeStar).

High-resolution metabolomics

LPS-primed BMDMs were stimulated with 5 mM ATP in the presence or absence of 10 μM JX06 for 45 min. Unstimulated macrophages were used as control. Macrophages were lysed, and polar metabolites were extracted using methanol and H_2O (80:20; HPLC Grade; Sigma-Aldrich) {Liu, 2015 #5193}. Extracts were dried under nitrogen gas, followed by liquid chromatography using Ultimate 3000 UHPLC (Dionex) coupled to high-resolution-mass spectrometry for metabolite profiling using the Q Exactive Plus-Mass spectrometer (QE-MS, Thermo Scientific) {Liu, 2014 #5194}. Commercial software Sieve 2.2 (Thermo Scientific) was using for peak extraction and integration. Liquid chromatography-mass spectrometry peak areas were normalized to sample protein mass measured by the BCA assay. Pathway analysis of metabolites was conducted using the MetaboAnalyst v.5.0.

Microscopy analysis

DIC imaging

DIC images of BMDMs were obtained using a Zeiss Axio Vert.A1 microscope with AxioCam ICc3 camera. Cells in more than 5 fields of a 20x objective were analyzed for cell size using NIH ImageJ software (NIH).

Confocal imaging

BMDMs seeded in a glass chamber slide were stained with 100 nM MitoTracker Deep Red (Invitrogen) for 15 min at 37 ^{o}C in dark. Macrophages were then washed and fixed with 4% paraformaldehyde. Nuclei were stained using DAPI. Confocal images were obtained with a FV1200 laser-scanning confocal microscope (Olympus).

Transmission electron microscopy (TEM) imaging

BMDMs were subjected to TEM imaging in the Wake Forest Baptist Health Electron Microscope Core Lab. Briefly, macrophages were fixed in 2.5% glutaraldehyde in 0.1M Millonig's phosphate buffer pH 7.3 for a

minimum of 1 h, wash with buffer, and post-fixed in % osmium tetroxide for 1 h. After dehydration, resin infiltration, and cure in a 70 ^{o}C oven overnight, cells were sectioned on a Reichert-Jung Ultracut E ultramicrotome. The sections were then stained with lead citrate and uranyl acetate and viewed with an FEI. Tecnai Spirit TEM was operating at 80 kV. Images were obtained with an AMT 2Vu CCD Camera. Mitochondrial morphology was analyzed on images with 4800x or 18500x magnification. More than 20 cells or 70 to 100 mitochondria per group were analyzed to quantify mitochondrial or cristae ultrastructure changes using NIH ImageJ software (NIH).

Mitochondrial ROS (mtROS) measurement

mtROS production in BMDMs was measured by MitoSOX (Fisher Scientific, no. M36008) staining (5 µM for 15 min at 37°C). Macrophages were washed with PBS and scraped off the dishes. Data were acquired with a FACSCanto II (BD Biosciences) and were analyzed with FlowJo analytical software (version 7.6.5, TreeStar).

Seahorse assays

2 x 10^5 BMDMs were plated into each well of Seahorse XF96 cell culture microplates (Agilent Technologies) and cultured overnight before treated with or without LPS plus ATP. Extracellular acidification rate (ECAR), oxygen consumption rate (OCR), and real-time ATP production rate in BMDMs were measured by using glycolysis stress kit, mitochondrial stress kit, and real-time ATP rate assay kit, respectively, with a Seahorse XF96 Extracellular Flux Analyzer (Agilent Technologies). 10 mM glucose, 1 µM oligomycin, 1.5 µM fluoro-carbonyl cyanide phenylhydrazone (FCCP), 100 nM rotenone plus 1 µM antimycin A, or 50 mM 2DG (all the compounds were from Agilent Technologies) were sequentially injected into the microplates according to the manufacturer's instructions. After the assay, 3 µM Hoechst (Life Technologies) was added to each well to stain nuclei for cell counting. Results were collected with Wave software version 2.6 (Agilent Technologies). Data were normalized to cell numbers.

siRNA transfection

50 nM control, PDHK1, PDHK2, PDHK4, or PDHE1a siRNA (Dharmacon, Lafayette, CO) was transfected into elicited peritoneal macrophages isolated from WT C57BL/6 mice with DharmaFECT 1 transfection reagent (Dharmacon, Lafayette, CO) according to the manufacturer's protocol. SiRNA transfection efficiency was quantified by qPCR or western blotting.

ELISA

Mouse IL-1β cytokine was measured in macrophage culture supernatants and mouse plasma using mouse IL-1β DuoSet ELISA Kit (R&D Systems) according to the manufacturer's instructions.

qPCR

Total RNA was isolated from macrophages using Trizol reagent (Thermo Fisher Scientific). cDNA was synthesized with Omniscript RT Kit (Qiagen). The relative mRNA expression level of each target gene was quantified by qPCR using KAPA SYBR fast qPCR master mix (Roche). Data were normalized to GAPDH and expressed relative to control unstimulated macrophages. The sequences of the primers are listed in Table S1.

Western Blotting

Macrophage cell lysates were lysed in radioimmunoprecipitation assay (RIPA) buffer containing protease inhibitor cocktails and PhosSTOP (Roche). Protein concentration was measured using the BCA Protein Assay Kit (Pierce). Primary antibodies used were anti-caspase-1 p20 (AdipoGen, no. AG-20B-0042; 1:1000), LC-3 (Novus Biologicals, no. NB100-2220; 1:500), P62 (Novus Biologicals, no. NBP1-48320; 1:4000), NLRP3 (Adipogen, no. AG-20B-0014; 1:1000), ASC (Adipogen, no. AG-25B-0006; 1:1000), PDHe1α (ThermoFisher, no. PA5-21536; 1:1000), p-AMPK (Cell Signaling, no. 50081s; 1:1000), p-ACC (Cell Signaling, no. 3661s; 1:750), TUFM (Novus Biologicals, no. CL2242; 1:500), GAPDH (Invitrogen, no. MA5-15738; 1:10,000), OPA1 (Cell Signaling, no. CST80471; 1:1000), p-DRP1 (Ser616) (Cell Signaling, no. 3455S; 1:500), p-TBK1 (Ser172) (Cell Signaling, no. CST5483; 1:1000); and β-actin (Sigma-Aldrich, no. A5441; 1:5000). Immunoblots were visualized with the Supersignal substrate system (Thermo Fisher Scientific), and chemiluminescence was captured using the ChemiDox MP imaging system (Bio-Rad) or an LSA-3000 imaging system (Fujifilm Life Science).

Statistics

Experiments were performed in triplicate or quadruplicate. At least two independent tests were performed for each assay except for high-resolution metabolomics analysis. Statistical analysis was performed using GraphPad Prism software 7 (GraphPad Software). Data are presented as the mean ± SEM unless indicated otherwise. Differences were compared with Student's t-test or one-way ANOVA with post hoc Tukey's multiple comparison test. Significant differences were regarded as $p < 0.05$, $p < 0.01$, $p < 0.001$, or $p<0.0001$, indicated in the figure legends.

Graphical Representations

Schematics and graphical abstract were created using BioRender online software.

References

AACHOUI, Y., LEAF, I. A., HAGAR, J. A., FONTANA, M. F., CAMPOS, C. G., ZAK, D. E., TAN, M. H., COTTER, P. A., VANCE, R. E., ADEREM, A. & MIAO, E. A. 2013. Caspase-11 protects against bacteria that escape the vacuole. *Science,* 339**,** 975-8.

BAMBOUSKOVA, M., POTUCKOVA, L., PAULENDA, T., KERNDL, M., MOGILENKO, D. A., LIZOTTE, K., SWAIN, A., HAYES, S., SHELDON, R. D., KIM, H., KAPADNIS, U., ELLIS, A. E., ISAGUIRRE, C., BURDESS, S., LAHA, A., AMARASINGHE, G. K., CHUBUKOV, V., RODDY, T. P., DIAMOND, M. S., JONES, R. G., SIMONS, D. M. & ARTYOMOV, M. N. 2021. Itaconate confers tolerance to late NLRP3 inflammasome activation. *Cell Rep,* 34**,** 108756.

BROZ, P., NEWTON, K., LAMKANFI, M., MARIATHASAN, S., DIXIT, V. M. & MONACK, D. M. 2010. Redundant roles for inflammasome receptors NLRP3 and NLRC4 in host defense against Salmonella. *J Exp Med,* 207**,** 1745-55.

BROZ, P., RUBY, T., BELHOCINE, K., BOULEY, D. M., KAYAGAKI, N., DIXIT, V. M. & MONACK, D. M. 2012. Caspase-11 increases susceptibility to Salmonella infection in the absence of caspase-1. *Nature,* 490**,** 288-91.

CAPPEL, D. A., DEJA, S., DUARTE, J. A. G., KUCEJOVA, B., IÑIGO, M., FLETCHER, J. A., FU, X., BERGLUND, E. D., LIU, T., ELMQUIST, J. K., HAMMER, S., MISHRA, P., BROWNING, J. D. & BURGESS, S. C. 2019. Pyruvate-Carboxylase-Mediated Anaplerosis Promotes Antioxidant Capacity by Sustaining TCA Cycle and Redox Metabolism in Liver. *Cell Metab,* 29**,** 1291-1305.e8.

CEREGHETTI, G. M., STANGHERLIN, A., MARTINS DE BRITO, O., CHANG, C. R., BLACKSTONE, C., BERNARDI, P. & SCORRANO, L. 2008. Dephosphorylation by calcineurin regulates translocation of Drp1 to mitochondria. *Proc Natl Acad Sci U S A,* 105**,** 15803-8.

CHEN, X., HE, W. T., HU, L., LI, J., FANG, Y., WANG, X., XU, X., WANG, Z., HUANG, K. & HAN, J. 2016. Pyroptosis is driven by non-selective gasdermin-D pore and its morphology is different from MLKL channel-mediated necroptosis. *Cell Res,* 26**,** 1007-20.

CHENG, S. C., SCICLUNA, B. P., ARTS, R. J., GRESNIGT, M. S., LACHMANDAS, E., GIAMARELLOS-BOURBOULIS, E. J., KOX, M., MANJERI, G. R., WAGENAARS, J. A., CREMER, O. L., LEENTJENS, J., VAN DER MEER, A. J., VAN DE VEERDONK, F. L., BONTEN, M. J., SCHULTZ, M. J., WILLEMS, P. H., PICKKERS, P., JOOSTEN, L. A., VAN DER POLL, T. & NETEA, M. G. 2016. Broad defects in the energy metabolism of leukocytes underlie immunoparalysis in sepsis. *Nat Immunol,* 17**,** 406-13.

COGLIATI, S., FREZZA, C., SORIANO, M. E., VARANITA, T., QUINTANA-CABRERA, R., CORRADO, M., CIPOLAT, S., COSTA, V., CASARIN, A., GOMES, L. C., PERALES-CLEMENTE, E., SALVIATI, L., FERNANDEZ-SILVA, P., ENRIQUEZ, J. A. & SCORRANO, L. 2013. Mitochondrial cristae shape determines respiratory chain supercomplexes assembly and respiratory efficiency. *Cell,* 155**,** 160-71.

CRUZ, C. M., RINNA, A., FORMAN, H. J., VENTURA, A. L., PERSECHINI, P. M. & OJCIUS, D. M. 2007. ATP activates a reactive oxygen species-dependent oxidative stress response and secretion of proinflammatory cytokines in macrophages. *J Biol Chem,* 282**,** 2871-9.

DANIELSKI, L. G., GIUSTINA, A. D., BONFANTE, S., BARICHELLO, T. & PETRONILHO, F. 2020. The NLRP3 Inflammasome and Its Role in Sepsis Development. *Inflammation,* 43**,** 24-31.

DERETIC, V. 2021. Autophagy in inflammation, infection, and immunometabolism. *Immunity,* 54**,** 437-453.

DUPONT, N., JIANG, S., PILLI, M., ORNATOWSKI, W., BHATTACHARYA, D. & DERETIC, V. 2011. Autophagy-based unconventional secretory pathway for extracellular delivery of IL-1β. *Embo j,* 30**,** 4701-11.

FANG, R., TSUCHIYA, K., KAWAMURA, I., SHEN, Y., HARA, H., SAKAI, S., YAMAMOTO, T., FERNANDES-ALNEMRI, T., YANG, R., HERNANDEZ-CUELLAR, E., DEWAMITTA, S. R., XU, Y., QU, H., ALNEMRI, E. S. & MITSUYAMA, M. 2011. Critical roles of ASC inflammasomes in caspase-1 activation and host innate resistance to Streptococcus pneumoniae infection. *J Immunol,* 187**,** 4890-9.

FERREIRA, A. C., SOARES, V. C., DE AZEVEDO-QUINTANILHA, I. G., DIAS, S., FINTELMAN-RODRIGUES, N., SACRAMENTO, C. Q., MATTOS, M., DE FREITAS, C. S., TEMEROZO, J. R., TEIXEIRA, L., DAMACENO HOTTZ, E., BARRETO, E. A., PÃO, C. R. R., PALHINHA, L., MIRANDA, M., BOU-HABIB, D. C., BOZZA, F. A., BOZZA, P. T. & SOUZA, T. M. L. 2021. SARS-CoV-2 engages inflammasome and pyroptosis in human primary monocytes. *Cell Death Discov,* 7**,** 43.

GEISLER, S., HOLMSTRÖM, K. M., SKUJAT, D., FIESEL, F. C., ROTHFUSS, O. C., KAHLE, P. J. & SPRINGER, W. 2010. PINK1/Parkin-mediated mitophagy is dependent on VDAC1 and p62/SQSTM1. *Nat Cell Biol,* 12**,** 119-31.

GONG, F., PENG, X., SANG, Y., QIU, M., LUO, C., HE, Z., ZHAO, X. & TONG, A. 2013. Dichloroacetate induces protective autophagy in LoVo cells: involvement of cathepsin D/thioredoxin-like protein 1 and Akt-mTOR-mediated signaling. *Cell Death Dis,* 4**,** e913.

HAGAR, J. A., POWELL, D. A., AACHOUI, Y., ERNST, R. K. & MIAO, E. A. 2013. Cytoplasmic LPS activates caspase-11: implications in TLR4-independent endotoxic shock. *Science,* 341**,** 1250-3.

HAGHIGHATDOOST, F., JABBARI, M. & HARIRI, M. 2019. The effect of L-carnitine on inflammatory mediators: a systematic review and meta-analysis of randomized clinical trials. *Eur J Clin Pharmacol,* 75**,** 1037-1046.

HARRIS, J., HARTMAN, M., ROCHE, C., ZENG, S. G., O'SHEA, A., SHARP, F. A., LAMBE, E. M., CREAGH, E. M., GOLENBOCK, D. T., TSCHOPP, J., KORNFELD, H., FITZGERALD, K. A. & LAVELLE, E. C. 2011. Autophagy controls IL-1beta secretion by targeting pro-IL-1beta for degradation. *J Biol Chem,* 286**,** 9587-97.

HENAO-MEJIA, J., ELINAV, E., THAISS, C. A. & FLAVELL, R. A. 2014. Inflammasomes and metabolic disease. *Annu Rev Physiol,* 76**,** 57-78.

HOOFTMAN, A., ANGIARI, S., HESTER, S., CORCORAN, S. E., RUNTSCH, M. C., LING, C., RUZEK, M. C., SLIVKA, P. F., MCGETTRICK, A. F., BANAHAN, K., HUGHES, M. M., IRVINE, A. D., FISCHER, R. & O'NEILL, L. A. J. 2020. The Immunomodulatory Metabolite Itaconate Modifies NLRP3 and Inhibits Inflammasome Activation. *Cell Metab*.

HUMPHRIES, F., SHMUEL-GALIA, L., KETELUT-CARNEIRO, N., LI, S., WANG, B., NEMMARA, V. V., WILSON, R., JIANG, Z., KHALIGHINEJAD, F., MUNEERUDDIN, K., SHAFFER, S. A., DUTTA, R., IONETE, C., PESIRIDIS, S., YANG, S., THOMPSON, P. R. & FITZGERALD, K. A. 2020. Succination inactivates gasdermin D and blocks pyroptosis. *Science,* 369**,** 1633-1637.

IYER, S. S., HE, Q., JANCZY, J. R., ELLIOTT, E. I., ZHONG, Z., OLIVIER, A. K., SADLER, J. J., KNEPPER-ADRIAN, V., HAN, R., QIAO, L., EISENBARTH, S. C., NAUSEEF, W. M., CASSEL, S. L. & SUTTERWALA, F. S. 2013. Mitochondrial cardiolipin is required for Nlrp3 inflammasome activation. *Immunity,* 39**,** 311-23.

JANG, S. & JAVADOV, S. 2020. OPA1 regulates respiratory supercomplexes assembly: The role of mitochondrial swelling. *Mitochondrion,* 51**,** 30-39.

JITRAPAKDEE, S., ST MAURICE, M., RAYMENT, I., CLELAND, W. W., WALLACE, J. C. & ATTWOOD, P. V. 2008. Structure, mechanism and regulation of pyruvate carboxylase. *Biochem J,* 413**,** 369-87.

KARPOVA, T., DANCHUK, S., KOLOBOVA, E. & POPOV, K. M. 2003. Characterization of the isozymes of pyruvate dehydrogenase phosphatase: implications for the regulation of pyruvate dehydrogenase activity. *Biochim Biophys Acta,* 1652**,** 126-35.

KAYAGAKI, N., STOWE, I. B., LEE, B. L., O'ROURKE, K., ANDERSON, K., WARMING, S., CUELLAR, T., HALEY, B., ROOSE-GIRMA, M., PHUNG, Q. T., LIU, P. S., LILL, J. R., LI, H., WU, J., KUMMERFELD, S., ZHANG, J., LEE, W. P., SNIPAS, S. J., SALVESEN, G. S., MORRIS, L. X., FITZGERALD, L., ZHANG, Y., BERTRAM, E. M., GOODNOW, C. C. & DIXIT, V. M. 2015. Caspase-11 cleaves gasdermin D for non-canonical inflammasome signalling. *Nature,* 526**,** 666-71.

KAYAGAKI, N., WARMING, S., LAMKANFI, M., VANDE WALLE, L., LOUIE, S., DONG, J., NEWTON, K., QU, Y., LIU, J., HELDENS, S., ZHANG, J., LEE, W. P., ROOSE-GIRMA, M. & DIXIT, V. M. 2011. Non-canonical inflammasome activation targets caspase-11. *Nature,* 479**,** 117-21.

KAYAGAKI, N., WONG, M. T., STOWE, I. B., RAMANI, S. R., GONZALEZ, L. C., AKASHI-TAKAMURA, S., MIYAKE, K., ZHANG, J., LEE, W. P., MUSZYNSKI, A., FORSBERG, L. S., CARLSON, R. W. & DIXIT, V. M. 2013. Noncanonical inflammasome activation by intracellular LPS independent of TLR4. *Science,* 341**,** 1246-9.

KELLY, B. & O'NEILL, L. A. 2015. Metabolic reprogramming in macrophages and dendritic cells in innate immunity. *Cell Res,* 25**,** 771-84.

KIM, M. J., YOON, J. H. & RYU, J. H. 2016. Mitophagy: a balance regulator of NLRP3 inflammasome activation. *BMB Rep,* 49**,** 529-535.

KLYUYEVA, A., TUGANOVA, A., KEDISHVILI, N. & POPOV, K. M. 2019. Tissue-specific kinase expression and activity regulate flux through the pyruvate dehydrogenase complex. *J Biol Chem,* 294**,** 838-851.

LAMKANFI, M. & DIXIT, V. M. 2012. Inflammasomes and their roles in health and disease. *Annu Rev Cell Dev Biol,* 28**,** 137-61.

LAMKANFI, M. & DIXIT, V. M. 2014. Mechanisms and functions of inflammasomes. *Cell,* 157**,** 1013-22.

LEE, S. J., JEONG, J. Y., OH, C. J., PARK, S., KIM, J. Y., KIM, H. J., DOO KIM, N., CHOI, Y. K., DO, J. Y., GO, Y., HA, C. M., CHOI, J. Y., HUH, S., HO JEOUNG, N., LEE, K. U., CHOI, H. S., WANG, Y., PARK, K. G., HARRIS, R. A. & LEE, I. K. 2015. Pyruvate Dehydrogenase Kinase 4 Promotes Vascular Calcification via SMAD1/5/8 Phosphorylation. *Sci Rep,* 5**,** 16577.

LEI, Y., WEN, H., YU, Y., TAXMAN, D. J., ZHANG, L., WIDMAN, D. G., SWANSON, K. V., WEN, K. W., DAMANIA, B., MOORE, C. B., GIGUÈRE, P. M., SIDEROVSKI, D. P., HISCOTT, J., RAZANI, B., SEMENKOVICH, C. F., CHEN, X. & TING, J. P. 2012. The mitochondrial proteins NLRX1 and TUFM form a complex that regulates type I interferon and autophagy. *Immunity,* 36**,** 933-46.

LI, X., LIU, J., HU, H., LU, S., LU, Q., QUAN, N., ROUSSELLE, T., PATEL, M. S. & LI, J. 2019. Dichloroacetate Ameliorates Cardiac Dysfunction Caused by Ischemic Insults Through AMPK Signal Pathway-Not Only Shifts Metabolism. *Toxicol Sci,* 167**,** 604-617.

LIN, G., HILL, D. K., ANDREJEVA, G., BOULT, J. K., TROY, H., FONG, A. C., ORTON, M. R., PANEK, R., PARKES, H. G., JAFAR, M., KOH, D. M., ROBINSON, S. P., JUDSON, I. R., GRIFFITHS, J. R., LEACH, M. O., EYKYN, T. R. & CHUNG, Y. L. 2014. Dichloroacetate induces autophagy in colorectal cancer cells and tumours. *Br J Cancer,* 111**,** 375-85.

LIN, J., CHEN, K., CHEN, W., YAO, Y., NI, S., YE, M., ZHUANG, G., HU, M., GAO, J., GAO, C., LIU, Y., YANG, M., ZHANG, Z., ZHANG, X., HUANG, J., CHEN, F., SUN, L., ZHANG, X., YU, S., CHEN, Y., JIANG, Y., WANG, S., YANG, X., LIU, K., ZHOU, H. M., JI, Z., DENG, H., HAQUE, M. E., LI, J., MI, L. Z., LI, Y. & YANG, Y. 2020. Paradoxical Mitophagy Regulation by PINK1 and TUFm. *Mol Cell,* 80**,** 607-620.e12.

LIU, T. F., VACHHARAJANI, V. T., YOZA, B. K. & MCCALL, C. E. 2012. NAD+-dependent sirtuin 1 and 6 proteins coordinate a switch from glucose to fatty acid oxidation during the acute inflammatory response. *J Biol Chem,* 287**,** 25758-69.

MAINALI, R., ZABALAWI, M., LONG, D., BUECHLER, N., QUILLEN, E., KEY, C. C., ZHU, X., PARKS, J. S., FURDUI, C., STACPOOLE, P. W., MARTINEZ, J., MCCALL, C. E. & QUINN, M. A. 2021. Dichloroacetate reverses sepsis-induced hepatic metabolic dysfunction. *Elife,* 10.

MANGAN, M. S. J., OLHAVA, E. J., ROUSH, W. R., SEIDEL, H. M., GLICK, G. D. & LATZ, E. 2018. Targeting the NLRP3 inflammasome in inflammatory diseases. *Nat Rev Drug Discov,* 17**,** 588-606.

MCCALL, C. E., ZABALAWI, M., LIU, T., MARTIN, A., LONG, D. L., BUECHLER, N. L., ARTS, R. J. W., NETEA, M., YOZA, B. K., STACPOOLE, P. W. & VACHHARAJANI, V. 2018. Pyruvate dehydrogenase complex stimulation promotes immunometabolic homeostasis and sepsis survival. *JCI Insight,* 3.

MEISER, J., KRÄMER, L., SAPCARIU, S. C., BATTELLO, N., GHELFI, J., D'HEROUEL, A. F., SKUPIN, A. & HILLER, K. 2016. Pro-inflammatory Macrophages Sustain Pyruvate Oxidation through Pyruvate Dehydrogenase for the Synthesis of Itaconate and to Enable Cytokine Expression. *J Biol Chem,* 291**,** 3932-46.

MEYERS, A. K. & ZHU, X. 2020. The NLRP3 Inflammasome: Metabolic Regulation and Contribution to Inflammaging. *Cells,* 9.

MILLS, E. L., KELLY, B., LOGAN, A., COSTA, A. S., VARMA, M., BRYANT, C. E., TOURLOMOUSIS, P., DABRITZ, J. H., GOTTLIEB, E., LATORRE, I., CORR, S. C., MCMANUS, G., RYAN, D., JACOBS, H. T., SZIBOR, M., XAVIER, R. J., BRAUN, T., FREZZA, C., MURPHY, M. P. & O'NEILL, L. A. 2016. Succinate Dehydrogenase Supports Metabolic Repurposing of Mitochondria to Drive Inflammatory Macrophages. *Cell,* 167**,** 457-470.e13.

MIN, B. K., PARK, S., KANG, H. J., KIM, D. W., HAM, H. J., HA, C. M., CHOI, B. J., LEE, J. Y., OH, C. J., YOO, E. K., KIM, H. E., KIM, B. G., JEON, J. H., HYEON, D. Y., HWANG, D., KIM, Y. H., LEE, C. H., LEE, T., KIM, J. W., CHOI, Y. K., PARK, K. G., CHAWLA, A., LEE, J., HARRIS, R. A. & LEE, I. K. 2019. Pyruvate Dehydrogenase Kinase Is a Metabolic Checkpoint for Polarization of Macrophages to the M1 Phenotype. *Front Immunol,* 10**,** 944.

MISAWA, T., SAITOH, T., KOZAKI, T., PARK, S., TAKAHAMA, M. & AKIRA, S. 2015. Resveratrol inhibits the acetylated alpha-tubulin-mediated assembly of the NLRP3-inflammasome. *Int Immunol,* 27**,** 425-34.

MISAWA, T., TAKAHAMA, M., KOZAKI, T., LEE, H., ZOU, J., SAITOH, T. & AKIRA, S. 2013. Microtubule-driven spatial arrangement of mitochondria promotes activation of the NLRP3 inflammasome. *Nat Immunol,* 14**,** 454-60.

MISHRA, P., CARELLI, V., MANFREDI, G. & CHAN, D. C. 2014. Proteolytic cleavage of Opa1 stimulates mitochondrial inner membrane fusion and couples fusion to oxidative phosphorylation. *Cell Metab,* 19**,** 630-41.

MOON, J. S., HISATA, S., PARK, M. A., DENICOLA, G. M., RYTER, S. W., NAKAHIRA, K. & CHOI, A. M. 2015a. mTORC1-Induced HK1-Dependent Glycolysis Regulates NLRP3 Inflammasome Activation. *Cell Rep,* 12**,** 102-15.

MOON, J. S., LEE, S., PARK, M. A., SIEMPOS, II, HASLIP, M., LEE, P. J., YUN, M., KIM, C. K., HOWRYLAK, J., RYTER, S. W., NAKAHIRA, K. & CHOI, A. M. 2015b. UCP2-induced fatty acid synthase promotes NLRP3 inflammasome activation during sepsis. *J Clin Invest,* 125**,** 665-80.

NA, Y. R., JUNG, D., SONG, J., PARK, J. W., HONG, J. J. & SEOK, S. H. 2020. Pyruvate dehydrogenase kinase is a negative regulator of interleukin-10 production in macrophages. *J Mol Cell Biol,* 12**,** 543-555.

NAKAHIRA, K., HASPEL, J. A., RATHINAM, V. A., LEE, S. J., DOLINAY, T., LAM, H. C., ENGLERT, J. A., RABINOVITCH, M., CERNADAS, M., KIM, H. P., FITZGERALD, K. A., RYTER, S. W. & CHOI, A. M. 2011. Autophagy proteins regulate innate immune responses by inhibiting the release of mitochondrial DNA mediated by the NALP3 inflammasome. *Nat Immunol,* 12**,** 222-30.

O'NEILL, L. A., KISHTON, R. J. & RATHMELL, J. 2016. A guide to immunometabolism for immunologists. *Nat Rev Immunol,* 16**,** 553-65.

PATEL, M. S., NEMERIA, N. S., FUREY, W. & JORDAN, F. 2014. The pyruvate dehydrogenase complexes: structure-based function and regulation. *J Biol Chem,* 289**,** 16615-23.

PEARCE, E. L. & PEARCE, E. J. 2013. Metabolic pathways in immune cell activation and quiescence. *Immunity,* 38**,** 633-43.

QUINTANA-CABRERA, R., QUIRIN, C., GLYTSOU, C., CORRADO, M., URBANI, A., PELLATTIERO, A., CALVO, E., VÁZQUEZ, J., ENRÍQUEZ, J. A., GERLE, C., SORIANO, M. E., BERNARDI, P. & SCORRANO, L. 2018. The cristae modulator Optic atrophy 1 requires mitochondrial ATP synthase oligomers to safeguard mitochondrial function. *Nat Commun,* 9**,** 3399.

RAMBOLD, A. S., COHEN, S. & LIPPINCOTT-SCHWARTZ, J. 2015. Fatty acid trafficking in starved cells: regulation by lipid droplet lipolysis, autophagy, and mitochondrial fusion dynamics. *Dev Cell,* 32**,** 678-92.

RATHINAM, V. A., VANAJA, S. K. & FITZGERALD, K. A. 2012a. Regulation of inflammasome signaling. *Nat Immunol,* 13**,** 333-42.

RATHINAM, V. A., VANAJA, S. K., WAGGONER, L., SOKOLOVSKA, A., BECKER, C., STUART, L. M., LEONG, J. M. & FITZGERALD, K. A. 2012b. TRIF licenses caspase-11-dependent NLRP3 inflammasome activation by gram-negative bacteria. *Cell,* 150**,** 606-19.

SANMAN, L. E., QIAN, Y., EISELE, N. A., NG, T. M., VAN DER LINDEN, W. A., MONACK, D. M., WEERAPANA, E. & BOGYO, M. 2016. Disruption of glycolytic flux is a signal for inflammasome signaling and pyroptotic cell death. *Elife,* 5**,** e13663.

SCHREPFER, E. & SCORRANO, L. 2016. Mitofusins, from Mitochondria to Metabolism. *Mol Cell,* 61**,** 683-694.

SHEN, L., YANG, Y., OU, T., KEY, C. C., TONG, S. H., SEQUEIRA, R. C., NELSON, J. M., NIE, Y., WANG, Z., BOUDYGUINA, E., SHEWALE, S. V. & ZHU, X. 2017. Dietary PUFAs attenuate NLRP3 inflammasome activation via enhancing macrophage autophagy. *J Lipid Res,* 58**,** 1808-1821.

SHI, C. S., SHENDEROV, K., HUANG, N. N., KABAT, J., ABU-ASAB, M., FITZGERALD, K. A., SHER, A. & KEHRL, J. H. 2012. Activation of autophagy by inflammatory signals limits IL-1beta production by targeting ubiquitinated inflammasomes for destruction. *Nat Immunol,* 13**,** 255-63.

SHI, J., ZHAO, Y., WANG, K., SHI, X., WANG, Y., HUANG, H., ZHUANG, Y., CAI, T., WANG, F. & SHAO, F. 2015. Cleavage of GSDMD by inflammatory caspases determines pyroptotic cell death. *Nature,* 526**,** 660-5.

SHIMADA, K., CROTHER, T. R., KARLIN, J., DAGVADORJ, J., CHIBA, N., CHEN, S., RAMANUJAN, V. K., WOLF, A. J., VERGNES, L., OJCIUS, D. M., RENTSENDORJ, A., VARGAS, M., GUERRERO, C., WANG, Y., FITZGERALD, K. A., UNDERHILL, D. M., TOWN, T. & ARDITI, M. 2012. Oxidized mitochondrial DNA activates the NLRP3 inflammasome during apoptosis. *Immunity,* 36**,** 401-14.

SMIRNOVA, E., GRIPARIC, L., SHURLAND, D. L. & VAN DER BLIEK, A. M. 2001. Dynamin-related protein Drp1 is required for mitochondrial division in mammalian cells. *Mol Biol Cell,* 12**,** 2245-56.

STACPOOLE, P. W. 2012. The pyruvate dehydrogenase complex as a therapeutic target for age-related diseases. *Aging Cell,* 11**,** 371-7.

STEARNS-KUROSAWA, D. J., OSUCHOWSKI, M. F., VALENTINE, C., KUROSAWA, S. & REMICK, D. G. 2011. The pathogenesis of sepsis. *Annu Rev Pathol,* 6**,** 19-48.

SUBRAMANIAN, N., NATARAJAN, K., CLATWORTHY, M. R., WANG, Z. & GERMAIN, R. N. 2013. The adaptor MAVS promotes NLRP3 mitochondrial localization and inflammasome activation. *Cell,* 153**,** 348-61.

SUGDEN, M. C. & HOLNESS, M. J. 2011. The pyruvate carboxylase-pyruvate dehydrogenase axis in islet pyruvate metabolism: Going round in circles? *Islets,* 3**,** 302-19.

SUN, W., XIE, Z., LIU, Y., ZHAO, D., WU, Z., ZHANG, D., LV, H., TANG, S., JIN, N., JIANG, H., TAN, M., DING, J., LUO, C., LI, J., HUANG, M. & GENG, M. 2015. JX06 Selectively Inhibits Pyruvate Dehydrogenase Kinase PDK1 by a Covalent Cysteine Modification. *Cancer Res,* 75**,** 4923-36.

SWAIN, A., BAMBOUSKOVA, M., KIM, H., ANDHEY, P. S., DUNCAN, D., AUCLAIR, K., CHUBUKOV, V., SIMONS, D. M., RODDY, T. P., STEWART, K. M. & ARTYOMOV, M. N. 2020. Comparative evaluation of itaconate and its derivatives reveals divergent inflammasome and type I interferon regulation in macrophages. *Nat Metab,* 2**,** 594-602.

SWANSON, K. V., DENG, M. & TING, J. P. 2019. The NLRP3 inflammasome: molecular activation and regulation to therapeutics. *Nat Rev Immunol,* 19**,** 477-489.

TANNAHILL, G. M., CURTIS, A. M., ADAMIK, J., PALSSON-MCDERMOTT, E. M., MCGETTRICK, A. F., GOEL, G., FREZZA, C., BERNARD, N. J., KELLY, B., FOLEY, N. H., ZHENG, L., GARDET, A., TONG, Z., JANY, S. S., CORR, S. C., HANEKLAUS, M., CAFFREY, B. E., PIERCE, K., WALMSLEY, S., BEASLEY, F. C., CUMMINS, E., NIZET, V., WHYTE, M., TAYLOR, C. T., LIN, H., MASTERS, S. L., GOTTLIEB, E., KELLY, V. P., CLISH, C., AURON, P. E., XAVIER, R. J. & O'NEILL, L. A. 2013. Succinate is an inflammatory signal that induces IL-1beta through HIF-1alpha. *Nature,* 496**,** 238-42.

WANG, Z., ZHAO, Q., NIE, Y., YU, Y., MISRA, B. B., ZABALAWI, M., CHOU, J. W., KEY, C. C., MOLINA, A. J., QUINN, M. A., FESSLER, M. B., PARKS, J. S., MCCALL, C. E. & ZHU, X. 2020. Solute Carrier Family 37 Member 2 (SLC37A2) Negatively Regulates Murine Macrophage Inflammation by Controlling Glycolysis. *iScience,* 23**,** 101125.

WIERSINGA, W. J., LEOPOLD, S. J., CRANENDONK, D. R. & VAN DER POLL, T. 2014. Host innate immune responses to sepsis. *Virulence,* 5**,** 36-44.

WOLF, A. J., REYES, C. N., LIANG, W., BECKER, C., SHIMADA, K., WHEELER, M. L., CHO, H. C., POPESCU, N. I., COGGESHALL, K. M., ARDITI, M. & UNDERHILL, D. M. 2016. Hexokinase Is an Innate Immune Receptor for the Detection of Bacterial Peptidoglycan. *Cell,* 166**,** 624-636.

WU, J., ZHAO, Y., PARK, Y. K., LEE, J. Y., GAO, L., ZHAO, J. & WANG, L. 2018. Loss of PDK4 switches the hepatic NF-κB/TNF pathway from pro-survival to pro-apoptosis. *Hepatology,* 68**,** 1111-1124.

XIE, M., YU, Y., KANG, R., ZHU, S., YANG, L., ZENG, L., SUN, X., YANG, M., BILLIAR, T. R., WANG, H., CAO, L., JIANG, J. & TANG, D. 2016. PKM2-dependent glycolysis promotes NLRP3 and AIM2 inflammasome activation. *Nat Commun,* 7**,** 13280.

ZHONG, Z., LIANG, S., SANCHEZ-LOPEZ, E., HE, F., SHALAPOUR, S., LIN, X. J., WONG, J., DING, S., SEKI, E., SCHNABL, B., HEVENER, A. L., GREENBERG, H. B., KISSELEVA, T. & KARIN, M. 2018. New mitochondrial DNA synthesis enables NLRP3 inflammasome activation. *Nature*.

ZHOU, R., YAZDI, A. S., MENU, P. & TSCHOPP, J. 2011. A role for mitochondria in NLRP3 inflammasome activation. *Nature,* 469**,** 221-5.

ZHU, X., LEE, J. Y., TIMMINS, J. M., BROWN, J. M., BOUDYGUINA, E., MULYA, A., GEBRE, A. K., WILLINGHAM, M. C., HILTBOLD, E. M., MISHRA, N., MAEDA, N. & PARKS, J. S. 2008. Increased cellular free cholesterol in macrophage-specific Abca1 knock-out mice enhances pro-inflammatory response of macrophages. *J Biol Chem,* 283**,** 22930-41.

ZHU, X., LONG, D., ZABALAWI, M., INGRAM, B., YOZA, B. K., STACPOOLE, P. W. & MCCALL, C. E. 2020. Stimulating pyruvate dehydrogenase complex reduces itaconate levels and enhances TCA cycle anabolic bioenergetics in acutely inflamed monocytes. *J Leukoc Biol*.

Figure 1

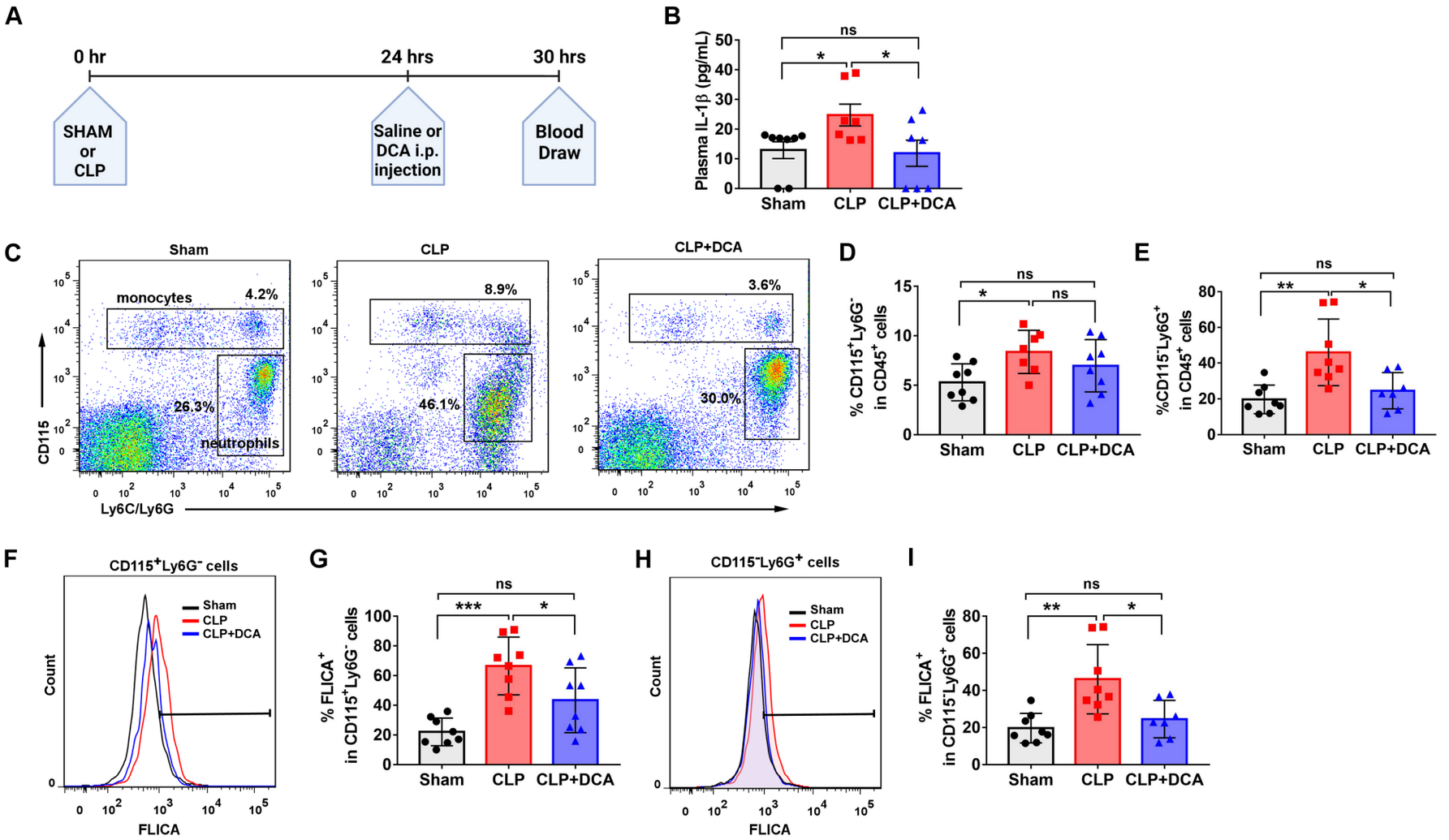
A
0 hr
24 hrs
30 hrs
SHAM or CLP
Saline or DCA i.p. injection
Blood Draw
B
Plasma IL-1β (pg/mL)
ns
*
*
Sham
CLP
CLP+DCA
C
Sham
CLP
CLP+DCA
monocytes
4.2%
26.3%
neutrophils
8.9%
46.1%
3.6%
30.0%
CD115
Ly6C/Ly6G
D
% CD115+Ly6G- in CD45+ cells
ns
*
ns
E
%CD115-Ly6G+ in CD45+ cells
ns
**
*
F
CD115+Ly6G- cells
Sham
CLP
CLP+DCA
Count
FLICA
G
% FLICA+ in CD115+Ly6G- cells
ns
***
*
H
CD115-Ly6G+ cells
Sham
CLP
CLP+DCA
Count
FLICA
I
% FLICA+ in CD115-Ly6G+ cells
ns
**
*

Figure 2

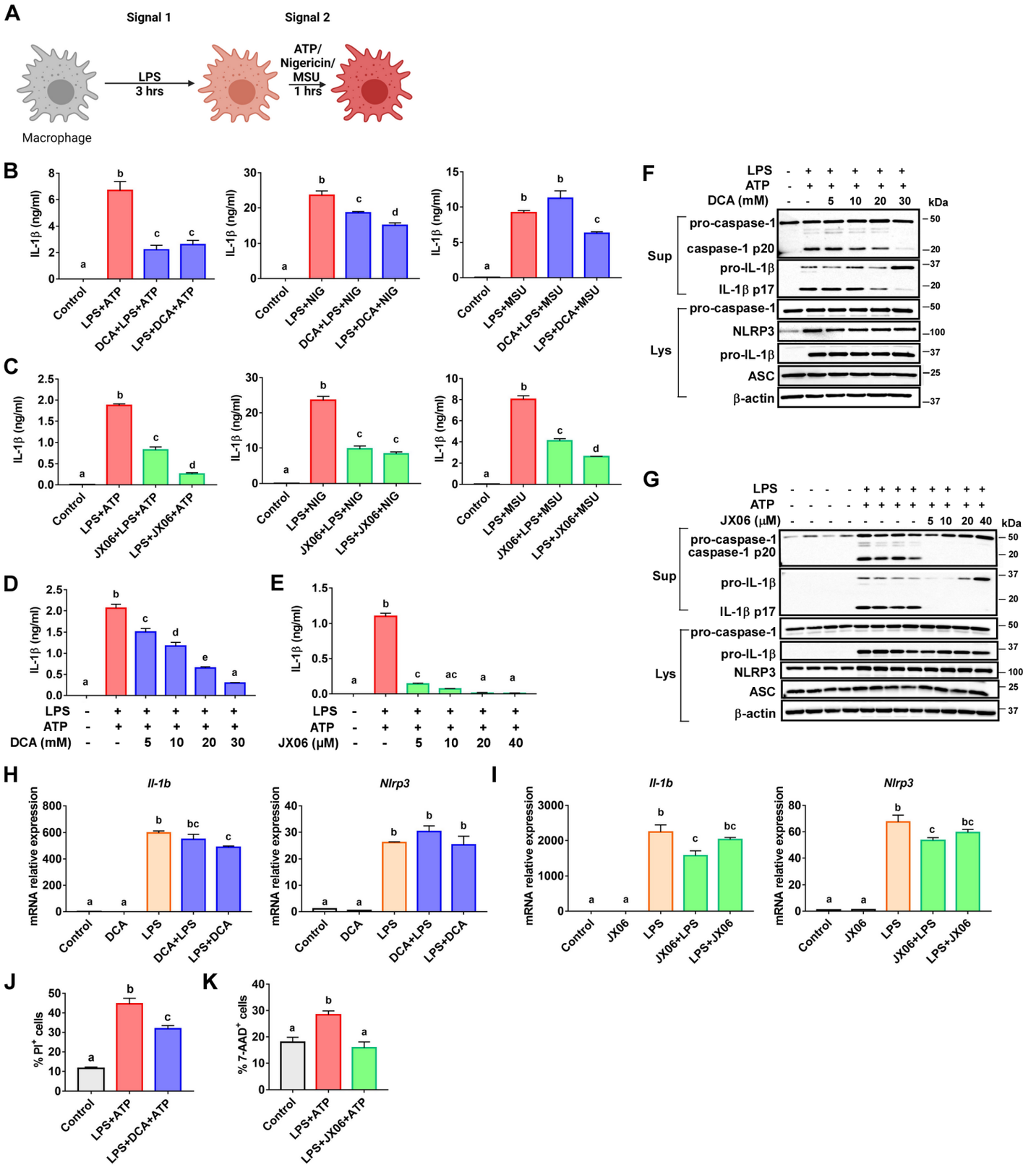
A
Signal 1
Signal 2
LPS
3 hrs
ATP/
Nigericin/
MSU
1 hrs
Macrophage
B
IL-1β (ng/ml)
Control
LPS+ATP
DCA+LPS+ATP
LPS+DCA+ATP
LPS+NIG
DCA+LPS+NIG
LPS+DCA+NIG
LPS+MSU
DCA+LPS+MSU
LPS+DCA+MSU
C
JX06+LPS+ATP
LPS+JX06+ATP
JX06+LPS+NIG
LPS+JX06+NIG
JX06+LPS+MSU
LPS+JX06+MSU
D
E
LPS
ATP
DCA (mM)
JX06 (μM)
F
Sup
Lys
pro-caspase-1
caspase-1 p20
pro-IL-1β
IL-1β p17
NLRP3
ASC
β-actin
kDa
G
H
Il-1b
Nlrp3
mRNA relative expression
DCA
LPS
DCA+LPS
LPS+DCA
I
JX06
JX06+LPS
LPS+JX06
J
% PI+ cells
K
% 7-AAD+ cells

Figure 3

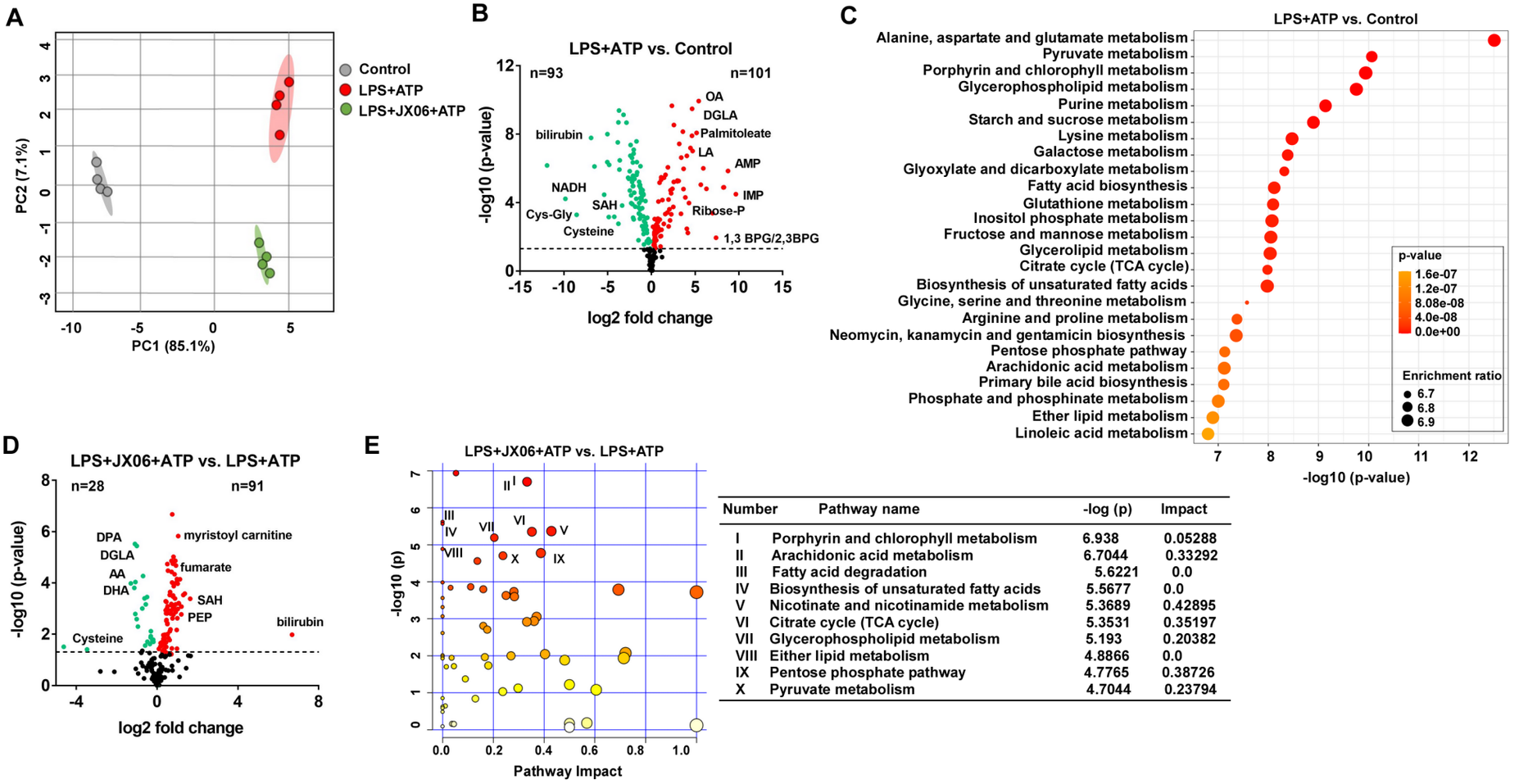

Number	Pathway name	-log (p)	Impact
I	Porphyrin and chlorophyll metabolism	6.938	0.05288
II	Arachidonic acid metabolism	6.7044	0.33292
III	Fatty acid degradation	5.6221	0.0
IV	Biosynthesis of unsaturated fatty acids	5.5677	0.0
V	Nicotinate and nicotinamide metabolism	5.3689	0.42895
VI	Citrate cycle (TCA cycle)	5.3531	0.35197
VII	Glycerophospholipid metabolism	5.193	0.20382
VIII	Either lipid metabolism	4.8866	0.0
IX	Pentose phosphate pathway	4.7765	0.38726
X	Pyruvate metabolism	4.7044	0.23794

Figure 4

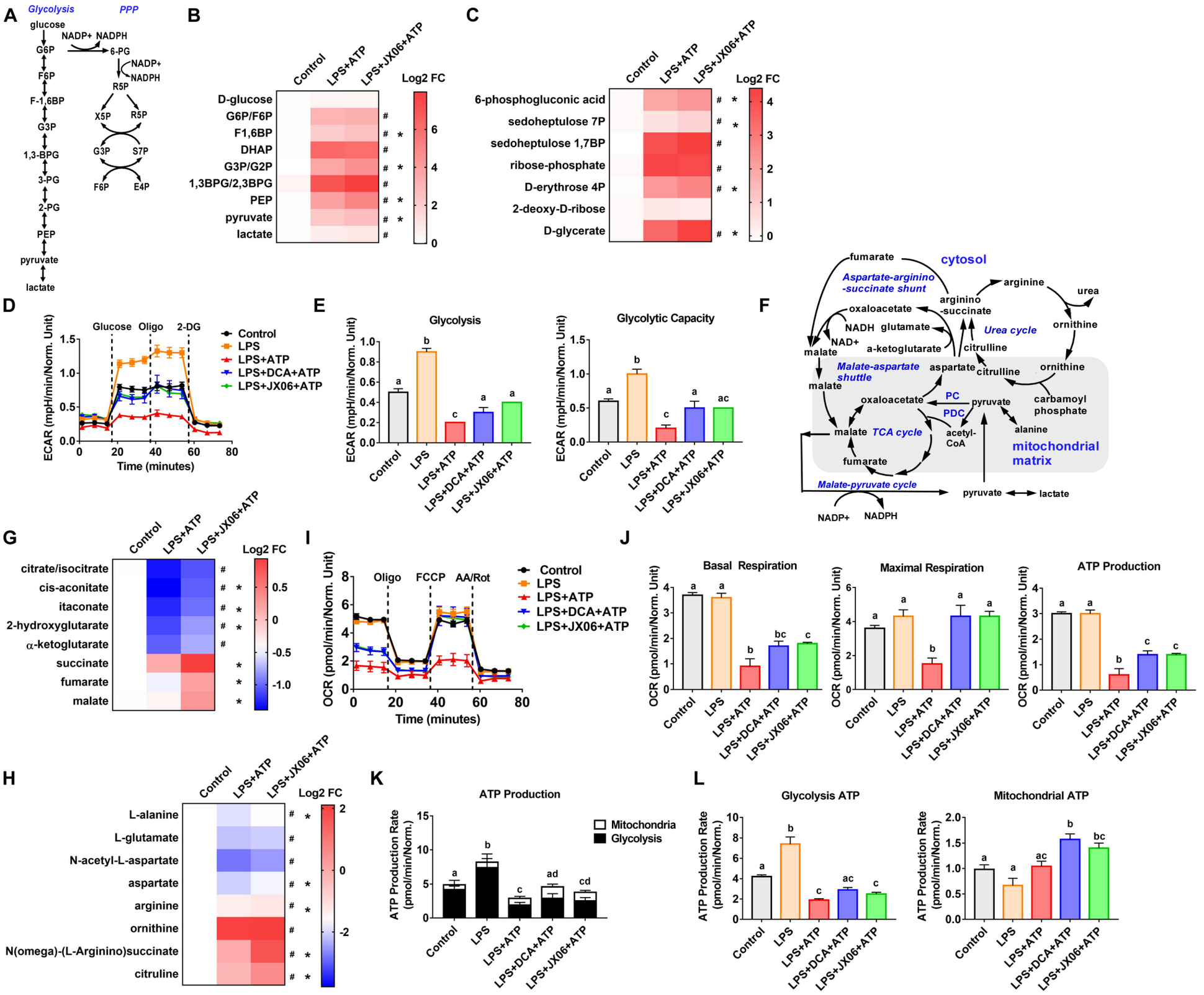
A
Glycolysis
PPP
glucose
G6P
F6P
F-1,6BP
G3P
1,3-BPG
3-PG
2-PG
PEP
pyruvate
lactate
NADP+ NADPH
6-PG
NADP+
NADPH
R5P
X5P
R5P
G3P
S7P
F6P
E4P
B
Control
LPS+ATP
LPS+JX06+ATP
Log2 FC
D-glucose
G6P/F6P
F1,6BP
DHAP
G3P/G2P
1,3BPG/2,3BPG
PEP
pyruvate
lactate
C
6-phosphogluconic acid
sedoheptulose 7P
sedoheptulose 1,7BP
ribose-phosphate
D-erythrose 4P
2-deoxy-D-ribose
D-glycerate
D
Glucose
Oligo
2-DG
Control
LPS
LPS+ATP
LPS+DCA+ATP
LPS+JX06+ATP
ECAR (mpH/min/Norm. Unit)
Time (minutes)
E
Glycolysis
Glycolytic Capacity
F
cytosol
fumarate
Aspartate-arginino -succinate shunt
arginine
urea
arginino -succinate
oxaloacetate
NADH
glutamate
Urea cycle
ornithine
NAD+
malate
a-ketoglutarate
citrulline
Malate-aspartate shuttle
aspartate
citrulline
ornithine
malate
oxaloacetate
PC
PDC
pyruvate
carbamoyl phosphate
malate
TCA cycle
acetyl-CoA
alanine
mitochondrial matrix
fumarate
Malate-pyruvate cycle
pyruvate
lactate
NADP+
NADPH
G
citrate/isocitrate
cis-aconitate
itaconate
2-hydroxyglutarate
α-ketoglutarate
succinate
fumarate
malate
I
Oligo
FCCP
AA/Rot
OCR (pmol/min/Norm. Unit)
Time (minutes)
J
Basal Respiration
Maximal Respiration
ATP Production
H
L-alanine
L-glutamate
N-acetyl-L-aspartate
aspartate
arginine
ornithine
N(omega)-(L-Arginino)succinate
citruline
K
ATP Production
Mitochondria
Glycolysis
ATP Production Rate (pmol/min/Norm.)
L
Glycolysis ATP
Mitochondrial ATP

Figure 5

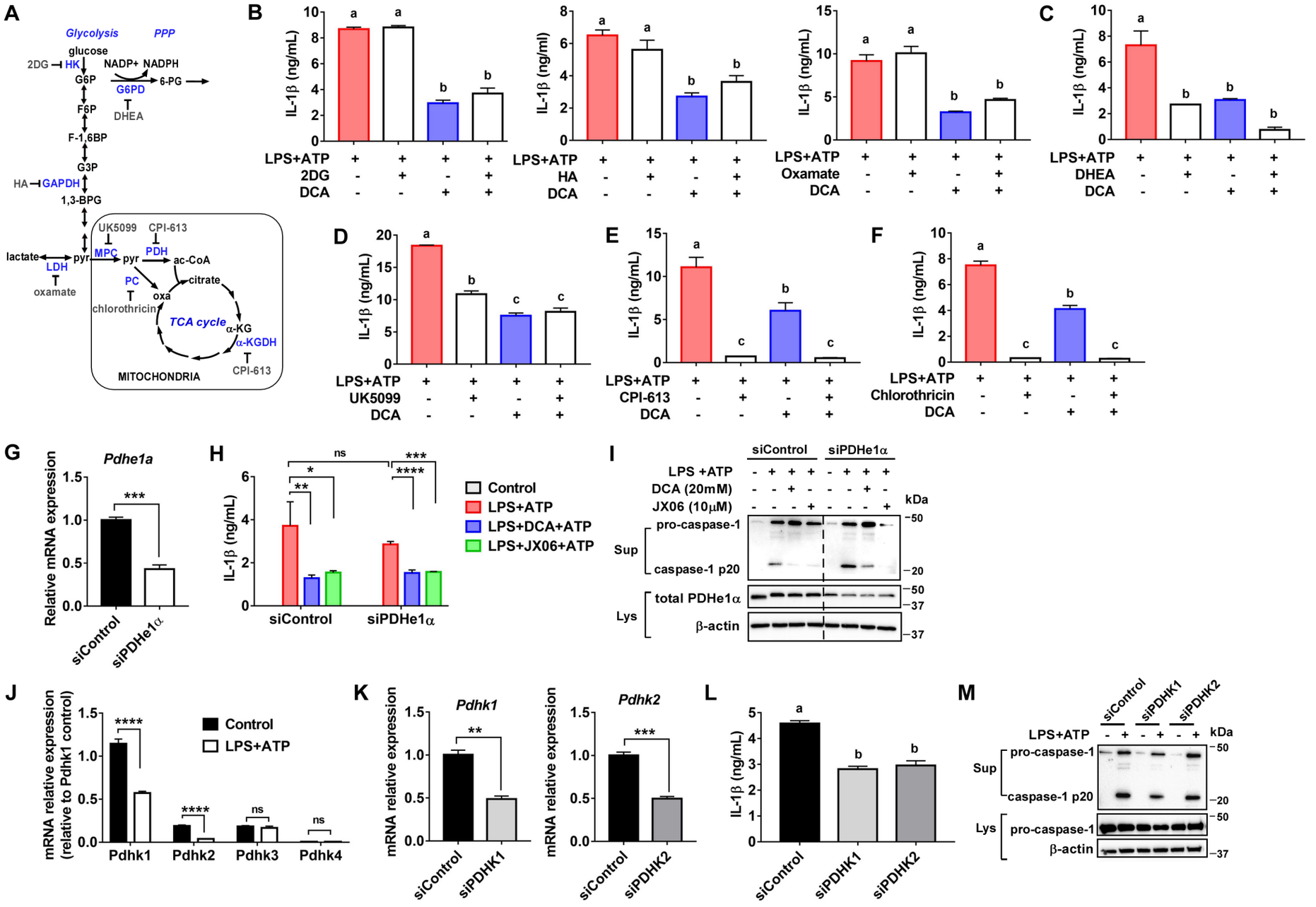
A
Glycolysis
PPP
glucose
2DG
HK
NADP+ NADPH
G6P
6-PG
G6PD
DHEA
F6P
F-1,6BP
G3P
HA
GAPDH
1,3-BPG
UK5099
CPI-613
lactate
pyr
MPC
pyr
PDH
ac-CoA
LDH
oxamate
PC
citrate
oxa
chlorothricin
TCA cycle
α-KG
α-KGDH
CPI-613
MITOCHONDRIA
B
IL-1β (ng/mL)
LPS+ATP
2DG
DCA
HA
Oxamate
C
DHEA
D
UK5099
E
CPI-613
F
Chlorothricin
G
Pdhe1a
Relative mRNA expression
siControl
siPDHe1α
H
IL-1β (ng/mL)
Control
LPS+ATP
LPS+DCA+ATP
LPS+JX06+ATP
I
siControl
siPDHe1α
LPS +ATP
DCA (20mM)
JX06 (10μM)
kDa
Sup
pro-caspase-1
caspase-1 p20
Lys
total PDHe1α
β-actin
J
mRNA relative expression (relative to Pdhk1 control)
Control
LPS+ATP
Pdhk1
Pdhk2
Pdhk3
Pdhk4
K
Pdhk1
Pdhk2
mRNA relative expression
siPDHK1
siPDHK2
L
IL-1β (ng/mL)
M
siPDHK1
siPDHK2

Figure 6

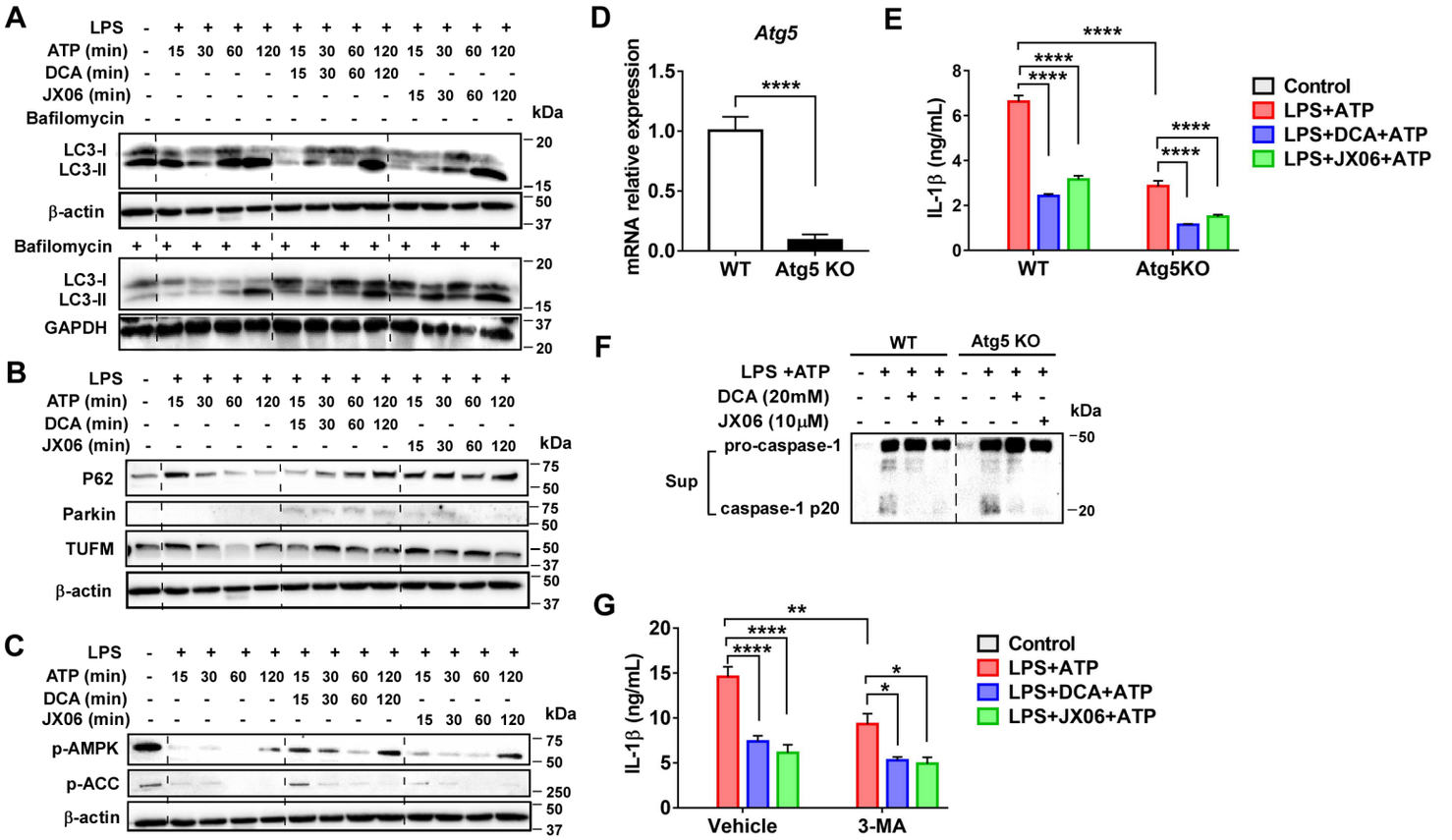
A
LPS
ATP (min)
DCA (min)
JX06 (min)
Bafilomycin
kDa
LC3-I
LC3-II
β-actin
GAPDH
B
P62
Parkin
TUFM
C
p-AMPK
p-ACC
D
Atg5
mRNA relative expression
WT
Atg5 KO
E
IL-1β (ng/mL)
Atg5KO
Control
LPS+ATP
LPS+DCA+ATP
LPS+JX06+ATP
F
LPS +ATP
DCA (20mM)
JX06 (10μM)
pro-caspase-1
Sup
caspase-1 p20
G
Vehicle
3-MA

Figure 7

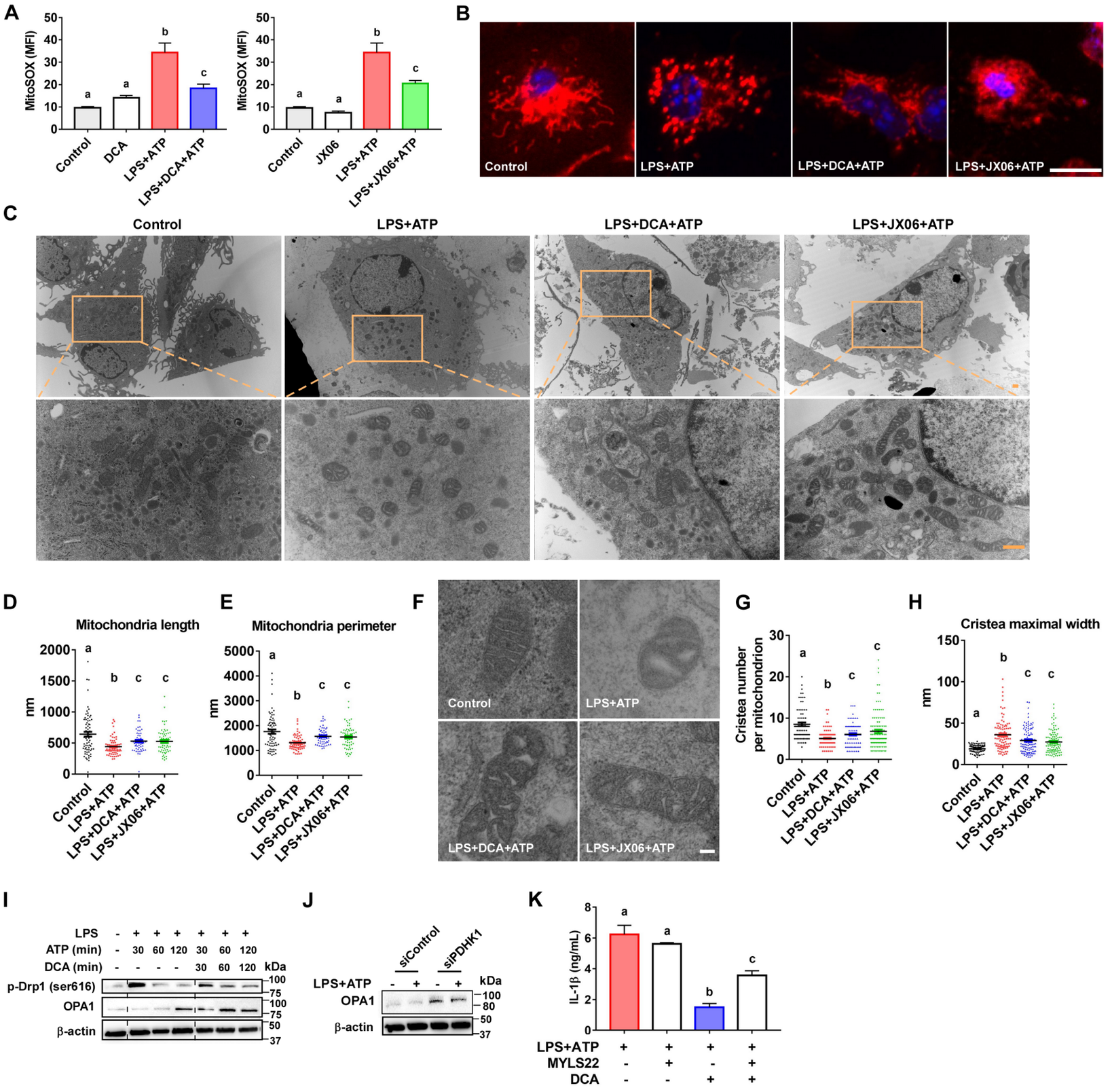
A
MitoSOX (MFI)
Control
DCA
LPS+ATP
LPS+DCA+ATP
JX06
LPS+JX06+ATP
B
Control
LPS+ATP
LPS+DCA+ATP
LPS+JX06+ATP
C
Control
LPS+ATP
LPS+DCA+ATP
LPS+JX06+ATP
D
Mitochondria length
nm
E
Mitochondria perimeter
nm
F
Control
LPS+ATP
LPS+DCA+ATP
LPS+JX06+ATP
G
Cristea number per mitochondrion
H
Cristea maximal width
nm
I
LPS
ATP (min)
DCA (min)
kDa
p-Drp1 (ser616)
OPA1
β-actin
J
siControl
siPDHK1
LPS+ATP
OPA1
β-actin
kDa
K
IL-1β (ng/mL)
LPS+ATP
MYLS22
DCA